16. Kamiyama T, Nakanishi K, Yokoo H, Kamachi H, Tahara M, Yamashita K, Taniguchi M, Shimamura T, Matsushita M, Todo S: **Perioperative management of hepatic resection toward zero mortality and morbidity: analysis of 793 consecutive cases in a single institution.** *J Am Coll Surg* 2010, **211**:443–449.
17. Dan YY, Aung MO, Lim SG: **The economics of treating chronic hepatitis B in Asia.** *Hepatol Int* 2008, **2**:284–295.
18. Ni YH, Chang MH, Hsu HY, Hsu HC, Chen CC, Chen WJ, Lee CY: **Hepatocellular carcinoma in childhood. Clinical manifestations and prognosis.** *Cancer* 1991, **68**:1737–1741.
19. Hernandez-Castillo E, Mondragon-Sanchez R, Garduno-Lopez AL, Gomez-Gomez E, Ruiz-Molina JM, Onate-Ocana LF, Bernal-Maldonado R: **Hepatocellular carcinoma in the youth. A comparative analysis with hepatocellular carcinoma in adulthood.** *Hepatogastroenterology* 2005, **52**:903–907.
20. Fan ST, Lo CM, Poon RT, Yeung C, Liu CL, Yuen WK, Lam CM, Ng KK, Chan SC: **Continuous improvement of survival outcomes of resection of hepatocellular carcinoma: a 20-year experience.** *Ann Surg* 2011, **253**:745–758.
21. Yang T, Lin C, Zhai J, Shi S, Zhu M, Zhu N, Lu JH, Yang GS, Wu MC: **Surgical resection for advanced hepatocellular carcinoma according to Barcelona Clinic Liver Cancer (BCLC) staging.** *J Cancer Res Clin Oncol* 2012, **138**:1121–1129.
22. Peng SY, Chen WJ, Lai PL, Jeng YM, Sheu JC, Hsu HC: **High alpha-fetoprotein level correlates with high stage, early recurrence and poor prognosis of hepatocellular carcinoma: significance of hepatitis virus infection, age, p53 and beta-catenin mutations.** *Int J Cancer* 2004, **112**:44–50.
23. Chuma M, Hige S, Kamiyama T, Meguro T, Nagasaka A, Nakanishi K, Yamamoto Y, Nakanishi M, Kohara T, Sho T, Yamamoto K, Horimoto H, Kobayashi T, Yokoo H, Matsushita M, Todo S, Asaka M: **The influence of hepatitis B DNA level and antiviral therapy on recurrence after initial curative treatment in patients with hepatocellular carcinoma.** *J Gastroenterol* 2009, **44**:991–999.
24. Li N, Lai EC, Shi J, Guo WX, Xue J, Huang B, Lau WY, Wu MC, Cheng SQ: **A comparative study of antiviral therapy after resection of hepatocellular carcinoma in the immune-active phase of hepatitis B virus infection.** *Ann Surg Oncol* 2010, **17**:179–185.
25. Ismail H, Broniszczak D, Kalicinski P, Markiewicz-Kijewska M, Teisseyre J, Stefanowicz M, Szymczak M, Dembowska-Baginska B, Kluge P, Perek D, Kosciesza A, Dzik E, Lembas A, Teisserye M: **Liver transplantation in children with hepatocellular carcinoma. Do Milan criteria apply to pediatric patients?** *Pediatr Transplant* 2009, **13**:682–692.
26. Romano F, Stroppa P, Bravi M, Casotti V, Lucianetti A, Guizzetti M, Sonzogni A, Colledan M, D'Antiga L: **Favorable outcome of primary liver transplantation in children with cirrhosis and hepatocellular carcinoma.** *Pediatr Transplant* 2011, **15**:573–579.
27. Saab S, McTigue M, Finn RS, Busuttil RW: **Sorafenib as adjuvant therapy for high-risk hepatocellular carcinoma in liver transplant recipients: feasibility and efficacy.** *Exp Clin Transplant* 2010, **8**:307–313.

doi:10.1186/1477-7819-11-52
Cite this article as: Shimada *et al.*: Clinicopathological characteristics and prognostic factors in young patients after hepatectomy for hepatocellular carcinoma. *World Journal of Surgical Oncology* 2013 11:52.

Surg Today (2013) 43:289–292
DOI 10.1007/s00595-012-0462-8

ORIGINAL ARTICLE

A rare point mutation in the Ras oncogene in hepatocellular carcinoma

Akinobu Taketomi · Ken Shirabe · Jun Muto · Shohei Yoshiya · Takashi Motomura · Yohei Mano · Tohru Ikegami · Tomoharu Yoshizumi · Kenji Sugio · Yoshihiko Maehara

Received: 16 May 2011 / Accepted: 17 May 2011 / Published online: 26 December 2012

Abstract
Purpose The Ras gene is one of the oncogenes most frequently detected in human cancers, and codes for three proteins (K-, N-, and H-Ras). The aim of this study was to examine the mutations in codons 12, 13 and 61 of the three Ras genes in cases of human hepatocellular carcinoma (HCC).
Methods Paired samples of HCC and corresponding non-malignant liver tissue were collected from 61 patients who underwent hepatectomy. A dot-blot analysis was used to analyze the products of the polymerase chain reaction (PCR) amplification of codons 12, 13, and 61 of K-, N- and H-Ras for mutations.
Results Only one mutation (K-Ras codon 13; Gly to Asp) was detected among the 61 patients. Interestingly, this patient had a medical history of surgery for both gastric cancer and right lung cancer. No mutations were found in codons 12 and 61 of K-Ras or codons 12, 13 and 61 of the N-Ras and H-Ras genes in any of the HCCs or corresponding non-malignant tissues.
Conclusions These findings indicated that the activation of Ras proto-oncogenes by mutations in codons 12, 13, and 61 does not play a major role in hepatocellular carcinogenesis.

Keywords Ras · Mutation · Hepatocellular carcinoma · Sorafenib

A. Taketomi (✉) · K. Shirabe · J. Muto · S. Yoshiya · T. Motomura · Y. Mano · T. Ikegami · T. Yoshizumi · K. Sugio · Y. Maehara
Department of Surgery and Science, Graduate School of Medical Sciences, Kyushu University, 3-1-1 Maidashi, Higashi-ku, Fukuoka, Japan
e-mail: taketomi@med.hokudai.ac.jp; taketomi@surg2.med.kyushu-u.ac.jp

Abbreviations

Asp	Asparagine
Glu	Glutamate
Gly	Glycine
HCC	Hepatocellular carcinoma
Lys	Lysine
PCR	Polymerase chain reaction
TTP	Time to progression
Val	Valine

Introduction

Hepatocellular carcinoma (HCC) is a global health problem, accounting for more than 80 % of all primary liver cancers, and is one of the most common malignancies worldwide [1]. Most patients with HCC also present with concomitant cirrhosis, which is the major clinical risk factor for hepatic cancer, and results from alcoholism or infection with the hepatitis B or hepatitis C virus. Primary liver malignancies (95 % of which are HCC) are the third and fifth leading causes of cancer death among males and females, respectively, in Japan [2]. Both liver resection and liver transplantation are potentially curative treatments for HCC [3–5]. Although other treatment options, including percutaneous radiofrequency ablation or chemolipiodolization are also available, there is no standard systemic therapy for advanced cases.

Sorafenib (BAY 43-9006, Nexavar) is a novel oral kinase inhibitor that targets multiple tyrosine kinases in vivo and in vitro, and is widely used for HCC [6]. The main targets of sorafenib are the receptor tyrosine kinase pathways which are frequently deregulated in cancer, such as the Ras pathway. The Ras pathway represents a dominant signaling network promoting cell proliferation and

survival. The binding of different growth factors (e.g. epidermal growth factor: EGF) to their receptors (e.g. epidermal growth factor receptor: EGFR) induces the activation of Ras, which in turn activates c-raf, MEK and ERK. Phosphorylated ERK in the nucleus activates transcription factors that regulate the expression of genes involved in cell proliferation and survival.

A phase II trial involving 137 patients with advanced HCC showed that sorafenib induced partial responses in less than 5 % of patients, but the observed median survival of 9.2 months with a median time to progression of 5.5 months was classified as evidence of potential clinical benefit, since the expected median survival of these patients is 6 months [7]. Consequently, a large phase III clinical trial (SHARP) was conducted in 602 patients with advanced HCC. The results showed a 31 % decrease in the risk of death, with a median survival of 10.6 months in the sorafenib arm versus 7.9 months for placebo [8]. In addition, sorafenib showed a significant benefit in terms of the time to progression (TTP) as assessed by independent radiological review, with a median TTP of 5.5 months for the sorafenib and 2.8 months for the placebo arm.

Because Ras is one of the targets of sorafenib, it is important to determine whether mutations in the Ras gene result in the activation of the Ras/MAPK pathway in human HCCs. However, the relationship between Ras mutations and human HCC has not been fully evaluated. The present study was designed to investigate K-, N- and H-Ras (*KRAS, NRAS, HRAS*) somatic mutations in human HCC.

Materials and methods

Patients and tumor samples

Tumor tissue samples were obtained from 61 Japanese patients who underwent surgical resection for HCC during the period between December 1989 and April 1992 in the Department of Surgery and Science, Kyushu University Hospital, Fukuoka, Japan. Surgically resected tissue samples were frozen at −80 °C immediately after resection and were stored until use in this study. Written informed consent was obtained from all patients examined, and the current study was approved by the Kyushu University ethics committee.

DNA preparation and detection of Ras point mutations

High molecular weight DNA was isolated from frozen tumor samples, as described elsewhere [9]. Selective amplification of the Ras gene sequence was done using a PCR technique. The nucleotide sequences of the primers used are listed in Table 1. The PCR was performed at

Table 1 Ras gene primers used in this study

Gene/codon	Length (bp)	Sequence	
KRAS/12, 13	108	Forward	GACTGAATATAAACTTGTGG
		Reverse	CTATTGTTGGATCATATTCG
KRAS/61	128	Forward	TTCCTACAGGAAGCAAGTAG
		Reverse	CACAAAGAAAGCCCTCCCCA
HRAS/12, 13	63	Forward	GACGGAATATAAGCTGGTGG
		Reverse	TGGATGGTCAGCGCACTCTT
HRAS/61	73	Forward	AGACGTGCCTGTTGGACATC
		Reverse	CGCATGTACTGGTCCCGCAT
NRAS/12, 13	109	Forward	GACTGAGTACAAACTGGTGG
		Reverse	CTCTATGGTGGGATCATATT
NRAS/61	103	Forward	GGTGAAACCTGTTTGTTGGA
		Reverse	ATACACAGAGGAAGCCTTCG

bp base pairs

96 °C to denature the DNA (1 min), at 55 °C (*NRAS*), 57 °C (*KRAS*), 62 °C (*HRAS*) to anneal the primer (30 s), and at 72 °C to synthesize DNA (10 s to 1 min) using Taq DNA polymerase for 35–40 cycles in a DNA thermal cycler (Perkin-Elmer-Cetus). Amplified DNA samples were spotted onto nylon membranes (Hybond N+) for the hybridization analysis. All of the DNA isolated from the 61 tumor samples and the corresponding non-malignant liver tissues were screened for activated point mutations in codons 12, 13, and 61 of all three Ras genes using an oligonucleotide specific for the different sequences. The filters were prehybridized for 1 h at 55 °C in solution A (3.0 M tetramethylammonium chloride, 50 mM Tris-HCl, 2 HIMEDTA, 0.1 % SDS, 5× Denhardt's solution, 100 fg/ml denatured herring sperm DNA), and hybridized for 1 h at 55 °C in the same solution with 5 pmol ^{32}P-labeled probe. These filters were washed twice in 0.3 M NaCl, 0.02 M NaH2PO4, 2 mM EDTA and 0.1 % SDS at room temperature for 5 min, and in solution A without Denhardt's solution and herring sperm DNA, once for 5 min at room temperature and twice for 10 min at 60 °C. These filters were then exposed to Kodak XAR5 film. Human cancer cell lines carrying Ras genes mutations were used as positive controls. The colon cancer cell lines: SW620 (*KRAS* codon 12 GTT:Val), LSI80 (*KRAS* codon 12 GAT:Asp), and LOVO (*KRAS* codon 13 GAC:Asp) were obtained from the Japanese Cancer Research Resources Bank, and KMS4 (*KRASs* codon 12 TGT:Cys) was provided by Dr. Sugio (Institution?).

Results

The age of the 61 patients ranged from 43 to 79 years (average, 64.1 years), and 46 were males and 15 were

females. The positive rate of hepatitis surface B antigen was 12.9 %, and the positive rate of anti-hepatitis C virus antibody was 72.7 %. The mean tumor size was 4.47 cm.

One of the 61 HCCs (1.6 %) carried a point mutation, which was a G to A transition at codon 13 of the *KRAS* gene (Fig. 1). DNA extracted from the corresponding non-malignant liver tissue had the normal codon, suggesting that mutational activation of K-ras was involved in the malignant transformation in this case. This patient was positive for anti-hepatitis C virus antibodies, and was classified to have Child-Pugh A disease. The diameter of this patient's tumor was 12 cm, and the tumor was composed of well to moderately differentiated hepatocellular carcinoma. Interestingly, this patient had undergone surgery for gastric cancer 18 years before and lung cancer 12 years before the surgery for HCC.

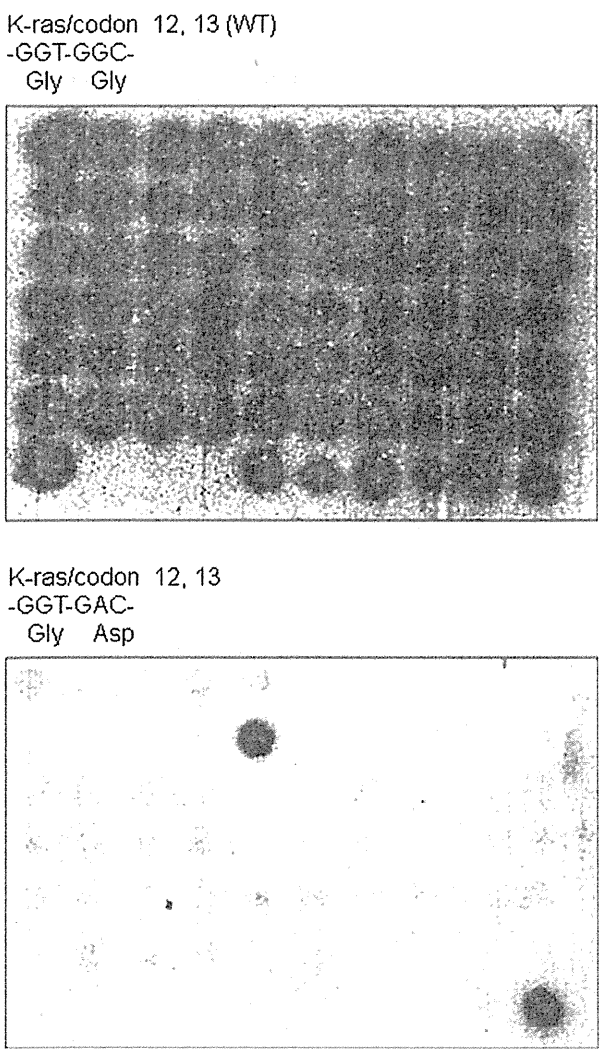

Fig. 1 Detection of a *KRAS* gene mutation in a patient with hepatocellular carcinoma. PCR-amplified DNA from 61 tumor samples was dotted onto nylon membranes and hybridized to a ^{32}P-labeled oligonucleotide probe. *WT* wild type *KRAS*

No mutational activation was found in codons 12 and 61 of *KRAS* or codons 12, 13 and 61 of the *NRAS* and *HRAS* genes in any of the HCCs or corresponding non-malignant tissue samples.

Discussion

This study examined 61 HCC tissues and their corresponding non-malignant liver tissues for a somatic mutation in codons 12, 13, and 61 of the *KRAS*, *HRAS*, or *NRAS* genes, which are known hot spots in various malignancies. However, the study showed the only one of the 61 HCCs (1.6 %) had a somatic mutation in codon 13 of the *KRAS* gene, indicating that Ras gene mutations do not appear to be related to the pathogenesis of most HCCs.

There have been several reports with small sample sizes regarding Ras gene mutations in HCC (Table 2). Most have reported that somatic mutations of the Ras gene in HCCs are uncommon, similar to the current study. Tsuda et al. [10] found only two tumors with Ras point mutations in surgically resected specimens from 30 HCC patients. In their patients, codon 12 of *KRAS* was altered from GGT, coding for Gly, to GTT, coding for Val in one case, and codon 61 of *NRAS* was altered from CAA, coding for Glu, to AAA, coding for Lys, in the other case. Tada et al. analyzed the mutations of the three Ras genes in 23 primary hepatic malignant tumors (12 hepatocellular carcinomas, nine cholangiocarcinomas, and two hepatoblastomas). Point mutations in *KRAS* codon 12 or *KRAS* codon 61 were found in 6 of the 9 cholangiocarcinomas. In contrast, there were no point mutations in any of 12 HCCs or two hepatoblastomas in codons 12, 13, or 61 of the Ras genes. The authors concluded that Ras gene mutations are not related to the pathogenesis of HCC, but play an important role in pathogenesis of cholangiocarcinoma.

Sorafenib is the first molecule with specific targets involved in the pathogenesis of HCC that has become available for routine clinical use. It is an orally applicable

Table 2 Reported Ras gene mutations in HCC patients

Author [references]	No. of patients	Ras gene mutation		
		KRAS	*NRAS*	*HRAS*
Tsuda et al. [10]	30	1 (codon 12)	1 (codon 61)	0
Tada et al. [14]	12	0	0	0
Ogata et al. [15]	19			2
Challen et al. [16]	19	1 (codon 61)	3 (codon 61)	0
Leon et al. [17]	12	1 (codon 61)	0	0
This study	61	1 (codon 13)	0	0

multi-kinase inhibitor that acts by blocking tumor cell proliferation and angiogenesis through the inhibition of serine/threonine kinases [11]. Sorafenib can increase survival by up to 3 months in patients with advanced HCC and acceptable liver function [8]. On the other hand, severe side effects have been reported with sorafenib, including hand-foot skin reactions or liver dysfunction [7, 8]. Therefore, it is important to identify prognostic markers and to establish the proper selection criteria for using sorafenib. Mutations of the Ras genes in cases of HCCs were systemically evaluated in this study because the Ras signaling pathway is the main target of sorafenib. The results indicated that mutational activation of Ras genes is uncommon in the pathogenesis of HCCs. Caraglia et al. [12] reported that the presence of phosphorylated ERK activity in peripheral blood mononuclear cells is valuable for predicting the response to sorafenib therapy in HCC patients. An in vitro study confirmed that phosphorylated ERK was a potential biomarker predicting the sensitivity of HCC to sorafenib [13]. Therefore, a mutation in the RAF/MEK/ERK pathway may be involved in the drug resistance to sorafenib, rather than a Ras mutation.

In summary, only one of 61 HCCs (1.6 %) in the present study carried a point mutation, which was a G to A transition in codon 13 of the *KRAS* gene. No mutational activation was found in codons 12 and 61 of *KRAS* or in codons 12, 13 and 61 of the *NRAS* or *HRAS* genes in any of the HCCs or corresponding non-malignant tissue samples. These findings suggested that Ras gene mutations are not related to the pathogenesis of most HCCs. The signaling pathways downstream of Ras should be examined to identify markers to predict a response to sorafenib.

Acknowledgments We thank Professor Brian Quinn for his review of this manuscript. No financial support was received for this work from any company. This study was supported in part by a grant from the Scientific Research Fund of the Ministry of Education of Japan.

Conflict of interest None of the authors has any conflict of interest.

References

1. El Serag HB, Rudolph KL. Hepatocellular carcinoma: epidemiology and molecular carcinogenesis. Gastroenterology. 2007;132:2557–76.
2. Okita K. Clinical aspects of hepatocellular carcinoma in Japan. Intern Med. 2006;45:229–33.
3. Taketomi A, Kitagawa D, Itoh S, Harimoto N, Yamashita Y, Gion T, et al. Trends in morbidity and mortality after hepatic resection for hepatocellular carcinoma: an institute's experience with 625 patients. J Am Coll Surg. 2007;204:580–7.
4. Taketomi A, Sanefuji K, Soejima Y, Yoshizumi T, Uhciyama H, Ikegami T, et al. Impact of des-gamma-carboxy prothrombin and tumor size on the recurrence of hepatocellular carcinoma after living donor liver transplantation. Transplantation. 2009;87:531–7.
5. Llovet JM, Schwartz M, Mazzaferro V. Resection and liver transplantation for hepatocellular carcinoma. Semin Liver Dis. 2005;25:181–200.
6. Llovet JM, Bruix J. Molecular targeted therapies in hepatocellular carcinoma. Hepatology. 2008;48:1312–27.
7. Abou Alfa GK, Schwartz L, Ricci S, Amadori D, Santoro A, Figer A, et al. Phase II study of sorafenib in patients with advanced hepatocellular carcinoma. J Clin Oncol. 2006;24:4293–300.
8. Llovet JM, Ricci S, Mazzaferro V, Hilgard P, Gane E, Blanc JF, et al. Sorafenib in advanced hepatocellular carcinoma. N Engl J Med. 2008;359:378–90.
9. Sugio K, Ishida T, Yokoyama H, Inoue T, Sugimachi K, Sasazuki T. Ras gene mutations as a prognostic marker in adenocarcinoma of the human lung without lymph node metastasis. Cancer Res. 1992;52:2903–6.
10. Tsuda H, Hirohashi S, Shimosato Y, Ino Y, Yoshida T, Terada M. Low incidence of point mutation of c-Ki-ras and N-ras oncogenes in human hepatocellular carcinoma. Jpn J Cancer Res. 1989;80:196–9.
11. Tanaka S, Arii S. Current status of molecularly targeted therapy for hepatocellular carcinoma: basic science. Int J Clin Oncol. 2010;15:235–41.
12. Caraglia M, Giuberti G, Marra M, Addeo R, Montella L, Murolo M, et al. Oxidative stress and ERK1/2 phosphorylation as predictors of outcome in hepatocellular carcinoma patients treated with sorafenib plus octreotide LAR. Cell Death Dis. 2011;2:e150.
13. Zhang Z, Zhou X, Shen H, Wang D, Wang Y. Phosphorylated ERK is a potential predictor of sensitivity to sorafenib when treating hepatocellular carcinoma: evidence from an in vitro study. BMC Med. 2009;7:41.
14. Tada M, Omata M, Ohto M. Analysis of ras gene mutations in human hepatic malignant tumors by polymerase chain reaction and direct sequencing. Cancer Res. 1990;50:1121–4.
15. Ogata N, Kamimura T, Asakura H. Point mutation, allelic loss and increased methylation of c-Ha-ras gene in human hepatocellular carcinoma. Hepatology. 1991;13:31–7.
16. Challen C, Guo K, Collier JD, Cavanagh D, Bassendine MF. Infrequent point mutations in codons 12 and 61 of ras oncogenes in human hepatocellular carcinomas. J Hepatol. 1992;14:342–6.
17. Leon M, Kew MC. Analysis of ras gene mutations in hepatocellular carcinoma in southern African blacks. Anticancer Res. 1995;15:859–61.

Original Paper

Pathobiology

Pathobiology 2013;80:146–154
DOI: 10.1159/000346196

Received: August 29, 2012
Accepted after revision: November 27, 2012
Published online: January 25, 2013

Tumor-Associated Macrophage Promotes Tumor Progression via STAT3 Signaling in Hepatocellular Carcinoma

Yohei Mano[a, b] Shinichi Aishima[a] Nobuhiro Fujita[c] Yuki Tanaka[a] Yuichiro Kubo[a] Takashi Motomura[b] Akinobu Taketomi[b] Ken Shirabe[b] Yoshihiko Maehara[b] Yoshinao Oda[a]

Departments of [a]Anatomic Pathology, [b]Surgery and Science, and [c]Clinical Radiology, Graduate School of Medical Sciences, Kyushu University, Fukuoka, Japan

Key Words
Hepatocellular carcinoma · STAT3 · Macrophage

Abstract
Objective: Signal transducer and activator of transcription 3 (STAT3) is activated in hepatocellular carcinoma (HCC), and tumor-associated macrophage plays an important role in tumor progression. Therefore, we examined STAT3 activation, cytokine expression and infiltration of tumor-associated macrophages in resected HCCs as well as the alteration of cell growth and migration by cytokine stimulation in HCC cell lines. ***Methods:*** Immunohistochemical staining of phosphorylated STAT3 (pSTAT3), CD163, interleukin (IL)-6, Ki-67 and Bcl-XL was performed for 101 cases of resected HCC, and correlations between pSTAT3 staining and clinicopathological findings were analyzed. In HCC cell lines (PLC/PRF/5 and Huh7), cell proliferation and migration by IL-6 stimulation and S3I-201 (STAT3 inhibitor) treatment were analyzed. ***Results:*** In HCC specimens, the pSTAT3-positive group showed high levels of α-fetoprotein ($p = 0.0276$), large tumor size ($p = 0.0092$), frequent intrahepatic metastasis ($p = 0.0214$), high Ki-67 ($p = 0.0002$) and Bcl-XL ($p = 0.0001$), poor prognosis ($p = 0.0234$), and high recurrence rate ($p = 0.0003$). CD163-positive cells were frequently observed in the pSTAT3-positive group ($p = 0.0013$). In two HCC cell lines, IL-6 stimulation promoted cell proliferation and migration via the STAT3 phosphorylation, and S3I-201 inhibited this activation. ***Conclusions:*** STAT3 activation was correlated with aggressive behavior of HCC and may be mediated via tumor-associated macrophage. We expect that STAT3 signaling and tumor-associated macrophages can be attractive therapeutic targets in HCC patients.

Introduction

Hepatocellular carcinoma (HCC) is the fifth most common cause of cancer in the world [1]. Although surgical therapies for HCC have progressed and outcomes of HCC have improved, HCC still often recurs after surgery [2, 3]. Sorafenib, one of the molecular targeted therapies, was reported to show activity against unresectable HCCs;

KARGER

Fax +41 61 306 12 34
E-Mail karger@karger.ch
www.karger.com

1015–2008/13/0803–0146$38.00/0

Accessible online at:
www.karger.com/pat

Yoshinao Oda, PhD
Department of Anatomic Pathology
Graduate School of Medical Sciences, Kyushu University
3-1-1 Maidashi, Higashi-ku, Fukuoka 812-8582 (Japan)
E-Mail oda@surgpath.med.kyushu-u.ac.jp

however, its survival advantage is only 3.7 months [4]. New therapeutic targets are required to improve the survival of patients with HCC.

Signal transducer and activator of transcription 3 (STAT3) is an important molecule in tumor progression [5]. STAT3 activation occurs via phosphorylation and dimerization of tyrosine residue (Tyr705), leading to nuclear entry, DNA binding and gene transcription. STAT3 was regarded as a critical transcription activator for cell cycle- or cell survival-related genes. Bcl-XL is an antiapoptotic protein transcribed by STAT3 activation [6]. Some cytokines such as interleukin (IL)-6 or IL-10 activate STAT3 signaling via their receptors [7]. Constitutive activation of STAT3 has been demonstrated to contribute to tumorigenesis in breast cancer [8], colon cancer [9], lung cancer [10], pancreatic cancer [11], prostate cancer [12], and melanoma [13]. In human HCC, STAT3 phosphorylation was also detected and related to tumor progression [14], angiogenesis [15] and tumorigenesis [16]. The tumor microenvironment is closely associated with the growth of tumor cells, and tumor-associated macrophages play an important role in tumor progression [17]. Macrophages are major inflammatory cells that infiltrate tumors; several studies have shown that high infiltration of tumor-associated macrophages was associated with tumor progression and metastasis [17–20] and predicts poor prognosis in patients with HCC [21]. Tumor-associated macrophages activate STAT3 in ovarian cancer [22] and glioblastoma [23]. However, the correlation between tumor-associated macrophages and STAT3 activation of HCC tumor cells is unknown. Therefore, we examined STAT3 activation, cytokine expression and infiltration of tumor-associated macrophages in resected HCCs and analyzed their association with clinicopathological findings. Alterations in cell growth and migration by cytokine stimulation and STAT3 inhibitor were also analyzed in HCC cell lines.

Materials and Methods

Patients and Samples

One hundred and one available paraffin-embedded specimens from patients with HCC who underwent hepatectomy between January 1997 and December 2001 in our institute were selected by reviewing their pathology data. Any patients undergoing previous or noncurative surgery were excluded. After the surgery, monthly measurement of the serum α-fetoprotein (AFP) level was performed. In addition, ultrasonography and dynamic CT were performed every 3 months. The postoperative survival period or recurrence was entered into the database immediately when a patient died or if recurrence was strongly suspected on diagnostic imaging such as CT or magnetic resonance imaging.

This study conformed to the ethical guidelines of the 1975 Declaration of Helsinki and was approved by the ethics committees of Kyushu University Hospital (grant No. 21-117). Informed consent was obtained from each patient included in the study.

Immunohistochemistry

Sections of resected specimens were fixed in 10% buffered formalin, embedded in paraffin and stained by Envision+ system and DAB kit (Dako, Glostrup, Denmark). Immunohistochemical stains were performed with antibodies of phosphorylated STAT3 (pSTAT3; Tyr 705; D3A7, 1:50; Cell Signaling Technology), CD163 (10D6, 1:200; Novocastra), IL-6 (rabbit polyclonal, 1:1,000; Abcam), Ki-67 (MIB-1, 1:200; Dako), and Bcl-XL (rabbit polyclonal, 1:200; Santa Cruz Biotechnology, Santa Cruz, Calif., US). Sections were pretreated before being incubated with primary antibodies in a microwave oven at 99°C for 20 min for pSTAT3, CD163, IL-6 and Bcl-XL or in a pressure cooker for 25 min for Ki-67.

Each slide was stained in serial sections and examined by two pathologists (Y.M. and S.A.). In nuclear staining of pSTAT3 and Ki-67 and in cytoplasm staining of Bcl-XL, the percent positive cells was estimated by count of 1,000 tumor cells in most staining areas (hot spots). Staining of CD163, a marker of tumor-associated macrophages [19, 22–25], and IL-6 was evaluated by estimating the total counts of cytoplasm or membrane at 3 high-power fields. The mean of nuclear pSTAT3-positive cells in HCCs was 10.7% (range 0–82.0), and pSTAT3 stain was classified into a positive (≥10.7% of tumor cell nuclei) and a negative group (<10.7% of tumor nuclei). Furthermore, in the cases of the pSTAT3-positive group (n = 36), the CD163-positive cells were counted separately in areas of pSTAT3-positive and pSTAT3-negative HCC cells.

For double staining of IL-6 and CD163, HCC specimens were boiled in 10 mM citrate buffer (pH 6.0) for 20 min and incubated with IL-6 primary antibody (1:1,000) at room temperature for 15 min. The sections were washed three times and incubated with anti-rabbit horseradish peroxidase-conjugated polymer at room temperature for 45 min; IL-6 was visualized by DAB kit. Next, the sections were boiled in 10 mM citrate buffer (pH 6.0) for 10 min, incubated with CD163 primary antibody (1:200) for 90 min and incubated with anti-mouse alkaline phosphatase-conjugated polymer at room temperature for 45 min. CD163 of the sections was visualized by New Fuchsin Substrate kit (Nichirei, Tokyo, Japan).

Cell Culture

Human HCC cell lines PLC/PRF/5 and Huh7 were obtained from Riken Bioresource Center, Tsukuba, Japan, and cultured in Dulbecco's modified Eagle's medium (DMEM) supplemented with 1 or 10% fetal bovine serum (FBS). PLC/PRF/5 and Huh7 cells were maintained in DMEM containing 1% FBS for 24 h prior to IL-6 (Peprotech, Rocky Hill, N.J., USA) stimulation. All in vitro experiments were done in triplicate.

Immunoblotting

Cellular proteins were solubilized in lysis buffer containing protease inhibitor and phosphatase inhibitor 30 min after stimulation with IL-6 (20 μg/ml). Equal amounts of protein were separated by SDS-PAGE and then transferred to the polyvinylidene fluoride membrane. Following blocking in Tris buffer containing 2% BSA, the membrane was stained with 1:1,000 dilution of anti-STAT3 (Cell Signaling Technology, Danvers, Mass., USA) and anti-pSTAT3 (Cell Signaling Technology) antibodies, then

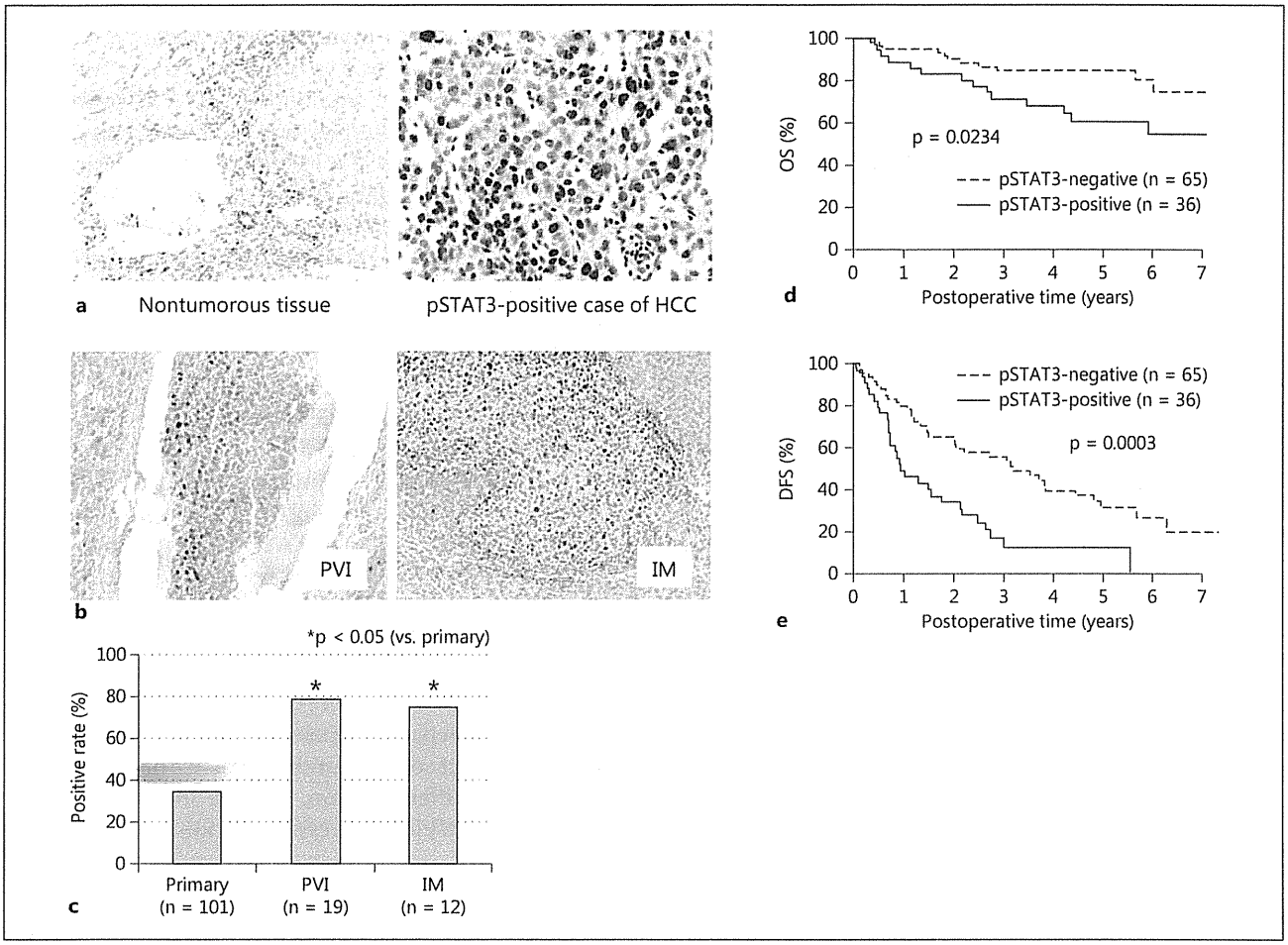

Fig. 1. Immunohistochemical staining of pSTAT3 in HCC. **a** pSTAT3 was expressed in the nucleus. In nontumorous tissue, endothelial cells, bile duct epithelial cells and inflammatory cells were stained by pSTAT3 (left panel). ×100. HCC cells were also stained (82.2%, right panel). ×100. **b** Tumor cells of PVI and IM stained by pSTAT3. ×200. **c** Comparison of pSTAT3 staining in primary HCC, tumor cells of PVI and IM. pSTAT3 staining was significantly prominent in tumor cells of PVI and IM compared with primary HCC ($p < 0.05$). **d**, **e** pSTAT3 expression correlated with poor prognosis. OS (**d**) and DFS (**e**) curves for pSTAT3-positive and pSTAT3-negative groups in patients with HCC (**d**, $p = 0.0234$; **e**, $p = 0.0003$; log-rank test).

washed and incubated with horseradish peroxidase-conjugated secondary antibody (Cell Signaling Technology). Bands were visualized by the enhanced chemiluminescence system (GE Healthcare, UK).

Cell Growth Assay

PLC/PRF/5 and Huh7 cells were seeded at a density of 5×10^4 cells/24-well plates and maintained in conditioned medium for 24 h before stimulation. Viable cells were counted by trypan blue stain 48 h after stimulation with IL-6 (25 ng/ml).

Wound-Healing Assay

PLC/PRF/5 and Huh7 cells were seeded at a density of 5×10^4 cells/6-well plates. Approximately 24 h later, when the cells were 100% confluent, a sterile 100-μl pipette tip was used to longitudinally scratch a constant-diameter strip in the confluent monolayer. The medium and cell debris were aspirated away and replaced by 2 ml of fresh DMEM containing 1% FBS with or without IL-6 (25 ng/ml). Photographs were taken at 0 and 48 h after wounding by phase-contrast microscopy. For statistical analysis, three randomly selected points along each wound were marked, and the horizontal distance between the migrating cells and the initial wound was measured 48 h later.

Inhibition of STAT3

In both cell growth and wound-healing assays, PLC/PRF/5 and Huh7 cells were cultured in DMEM containing 1% FBS and IL-6 (25 ng/ml) with or without 100 nM S3I-201 (NSC 74859; Santa Cruz Biotechnology). S3I-201 was treated 30 min before IL-6 stimulation. DMSO was used for control.

Table 1. Comparison of pSTAT3 expression and clinicopathological findings

pSTAT3 expression	pSTAT3 negative (n = 65)	pSTAT3 positive (n = 36)	p value
Clinical features			
Sex, male/female	55/10	26/10	0.0849
Age, years	63.9±7.3	63.6±9.5	0.8726
HBsAg, +/–	14/51	8/28	0.9922
HCV Ab, +/–	42/23	23/13	0.9798
Cirrhosis	22/43	14/22	0.4990
AFP, ng/ml	852.4±308†	20,673.4±11,688†	0.0276*
DCP, mAU/ml	2,798.2±1,179.1†	6,278.4±3,184.7†	0.2217
Pathological features			
Tumor size, cm	3.7±2.2	5.1±3.2	0.0092*
Differentiation, poor/well and moderate	19/46	16/20	0.1253
Capsule formation	41/24	26/10	0.4619
Infiltration to the capsule	33/32	23/13	0.1681
Portal venous invasion, +/–	30/35	24/12	0.0687
Hepatic venous invasion, +/–	15/50	12/24	0.3031
Intrahepatic metastasis, +/–	18/47	18/18	0.0214*
MIB-1 LI, %	3.5±0.5	10.2±2.2	0.0002*
Bcl-XL, %	13.0±1.5	25.2±2.0	0.0001*

HBsAg = Hepatitis B surface antigen; HCV Ab = hepatitis C virus antibody; DCP = des-γ-carboxy prothorombin. * $p < 0.05$.

Statistical Analysis

Statistical analysis was carried out using Microsoft Excel software and JMP software (SAS Institute, Cary, N.C., USA). Comparison between pSTAT3 staining and clinicopathological findings or staining of other antibodies was evaluated by Pearson's χ^2, Fisher's exact tests and the Mann-Whitney U test. Patient survival analysis including overall survival (OS) and disease-free survival (DFS) was calculated by the Kaplan-Meier method; differences were evaluated by the log-rank test. For multivariate analysis, the Cox proportional hazard model was used. Two-sided Student's t test was applied for analysis of in vitro data. Statistical analyses were considered significant at a p value <0.05.

Results

pSTAT3 Expression in Clinical Samples

pSTAT3 was stained in the nuclei of HCC cells, normal endothelial cells, some bile duct epithelial cells and inflammatory cells. pSTAT3 nuclear staining in HCC cells is displayed in figure 1a. The mean percentage of nuclear pSTAT3-positive cells in HCCs was 10.7% (range 0–82.0). The number of pSTAT3-positive and pSTAT3-negative samples was 36 and 65, respectively. We also examined pSTAT3 staining at the lesions of 19 portal venous invasions (PVIs) and 12 intrahepatic metastases (IMs) in 101 cases. Fifteen of 19 PVIs (78.9%) and 9 of 12 (75.0%) IMs were defined as pSTAT3-positive cases (fig. 1b). Positive rates in both lesions were significantly higher than those in the primary lesions (35.6%; $p < 0.05$; fig. 1c).

Comparison of pSTAT3 Expression and Clinicopathological Findings

A comparison of clinicopathological findings in pSTAT3-positive and pSTAT3-negative groups is summarized in table 1. The pSTAT3-positive group showed higher AFP ($p = 0.0276$), larger tumor size ($p = 0.0092$), more frequent IMs ($p = 0.0214$), a higher Ki-67 labeling index (LI; $p = 0.0002$), and more Bcl-XL-positive cells ($p = 0.0001$) than the pSTAT3-negative group, whereas no significant differences were noted with respect to sex, age, infection of hepatitis viruses, liver cirrhosis, PIVKA II (proteins induced by vitamin K absence or antagonist II), histological differentiation, capsule formation, infiltration to the capsule, and vessel invasion.

Survival Analysis after Surgery

The median follow-up period was 1,391 days (range 36–3,289). pSTAT3 expression was significantly correlated with OS and DFS ($p = 0.0234$ and 0.0003, respectively; fig. 1d, e). Univariate analyses indicated that high AFP (>100 ng/ml), large tumor size (>5 cm), PVIs and IMs were prognostic factors for OS and male sex, hepatitis C virus infection, high AFP (>100 ng/ml) and IMs for DFS (table 2). Multivariate proportional hazard models revealed that high AFP and IMs were independent prognostic factors for OS and pSTAT3 expression and high AFP for DFS (table 2).

Tumor-Associated Macrophage Localization and pSTAT3 Expression of HCCs

CD163-positive cells were localized around the pSTAT3-positive HCC cells (fig. 2a). Figure 2b shows the boxplots of CD163-positive cells (mean ± SD: pSTAT3-negative group, 28.5 ± 15.4; pSTAT3-positive group, 42.6 ± 26.6). The pSTAT3-positive group (n = 36) showed statistically higher CD163-positive cells ($p = 0.0013$; fig. 2b) than the pSTAT3-negative group (n = 65). Furthermore, we analyzed the localization of CD163-posi-

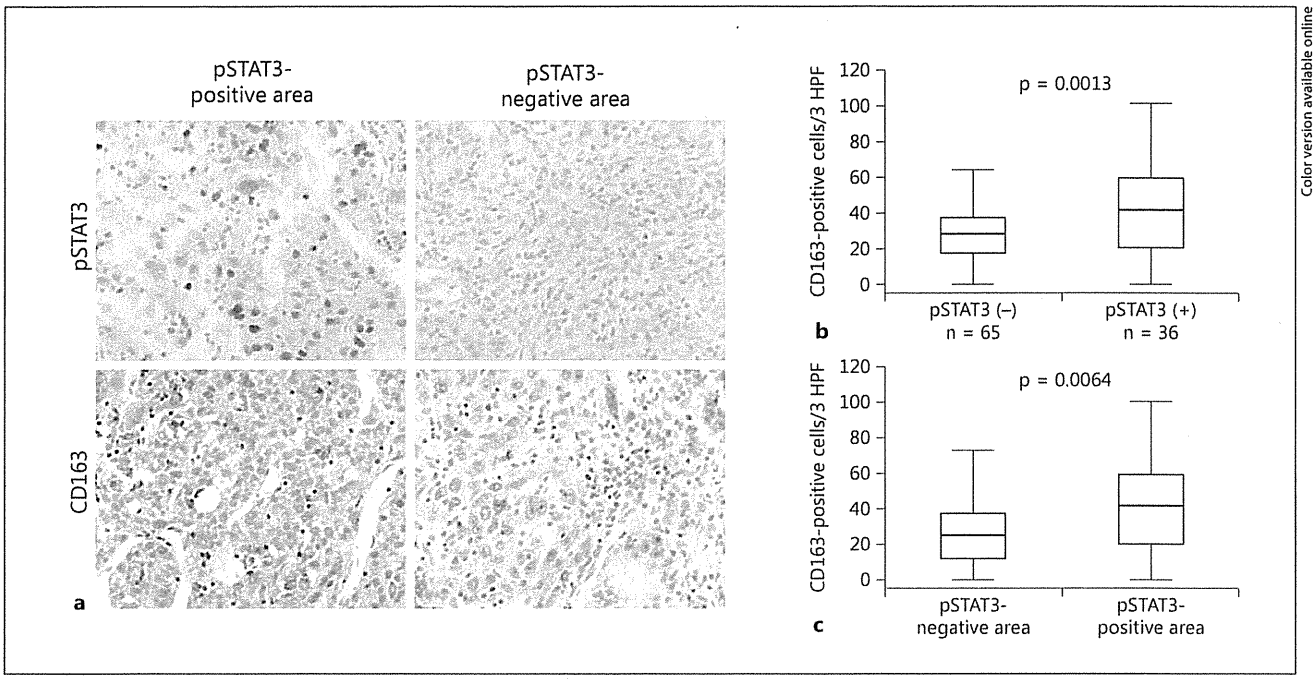

Fig. 2. Tumor-associated macrophages correlated with pSTAT3 expression in HCC. **a** Immunohistochemical staining of pSTAT3 and CD163 in the pSTAT3-positive and pSTAT3-negative area. ×200. **b** Counts of CD163-positive cells between pSTAT3-positve and pSTAT3-negative groups. **c** Counts of CD163-positive cells in areas of pSTAT3-positive and pSTAT3-negative HCC cells existed in the pSTAT3-positive group. HPF = High-power field.

Table 2. Survival analysis after surgery

Variable	Univariate analysis of OS	Multivariate analysis of OS		
	p value	hazard ratio	95% CI	p value
pSTAT3 positive	0.0234*	1.104	0.465–2.683	0.8236
AFP >100 ng/ml	0.0005*	2.968	1.294–7.026	0.0103*
Tumor size >5 cm	0.0246*	1.489	0.610–3.578	0.3755
Portal venous invasion	0.0422*	1.568	0.629–4.1265	0.3367
Intrahepatic metastasis	0.0022*	2.668	1.186–6.194	0.0177*
Variable	Univariate analysis of DFS	Multivariate analysis of DFS		
	p value	hazard ratio	95% CI	p value
pSTAT3 positive	0.0003*	1.851	1.066–3.201	0.0288*
Sex, male	0.0267*	0.978	0.515–1.790	0.9431
HCV Ab (+)	0.0158*	1.672	0.948–3.096	0.0767
AFP >100 ng/ml	0.0002*	2.070	1.218–3.476	0.0076*
Intrahepatic metastasis	0.0012*	1.702	0.964–3.012	0.0664

CI = Confidence interval; HCV Ab = hepatitis C virus antibody. * $p < 0.05$.

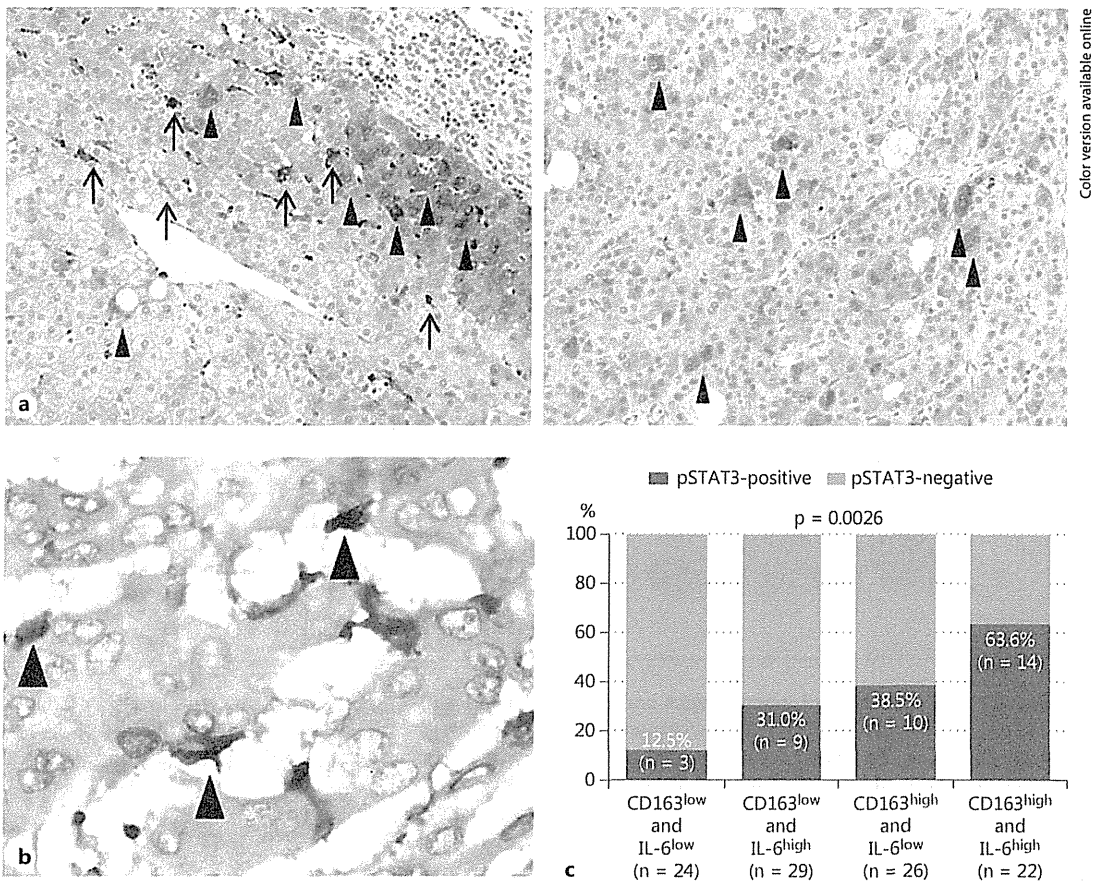

Color version available online

Fig. 3. Tumor-associated macrophages expressed IL-6. **a** Immunohistochemical staining of IL-6 in HCC. ×200. Not only macrophages (arrows, left panel) but also some hepatocytes (arrowheads, left panel) and some tumor cells (arrowheads, right panel) showed immunoreactivities for IL-6. **b** Double staining of IL-6 (red) and CD163 (brown). ×400. Double-positive cells (arrowheads) were frequently seen in the tumor. **c** Correlation between pSTAT3-positive and IL-6/CD163-positive staining.

tive cells in areas where pSTAT3-positive and pSTAT3-negative HCC cells existed in the pSTAT3-positive group (n = 36), and figure 2c shows the boxplots of the analyses (mean ± SD: pSTAT3-negative area, 27.7 ± 17.9; pSTAT3-positive area, 42.6 ± 26.6). In the pSTAT3-positive group, CD163-positive cells in areas where pSTAT3-positive HCC cells existed were statistically higher than in those where pSTAT3-negative HCC cells existed (p = 0.0064; fig. 2c).

Cytokine Expression of Macrophages

IL-6 was stained in some macrophages, HCC cells and normal hepatocytes (fig. 3a). According to the double staining of CD163 and IL-6, CD163-positive cells (tumor-associated macrophages) expressed IL-6 (fig. 3b). We divided them into two by the median values of positive macrophages of IL-6 and CD163, and thereby classified the 101 cases into four groups such as $CD163^{low}$ and $IL\text{-}6^{low}$, $CD163^{low}$ and $IL\text{-}6^{high}$, $CD163^{high}$ and $IL\text{-}6^{low}$, and $CD163^{high}$ and $IL\text{-}6^{high}$. HCCs containing high infiltration of IL-6- and CD163-positive macrophages exhibited a significantly higher rate of positive staining for pSTAT3 (fig. 3c).

IL-6 Stimulates Cell Proliferation and Migration of Human HCC Cell Lines

IL-6 stimulation increased the levels of pSTAT3 in both PLC/PRF/5 and Huh7 HCC cell lines (fig. 4a). IL-6 stimulation resulted in higher proliferation (fig. 4b) and greater migration distance (fig. 4c) versus control. S3I-

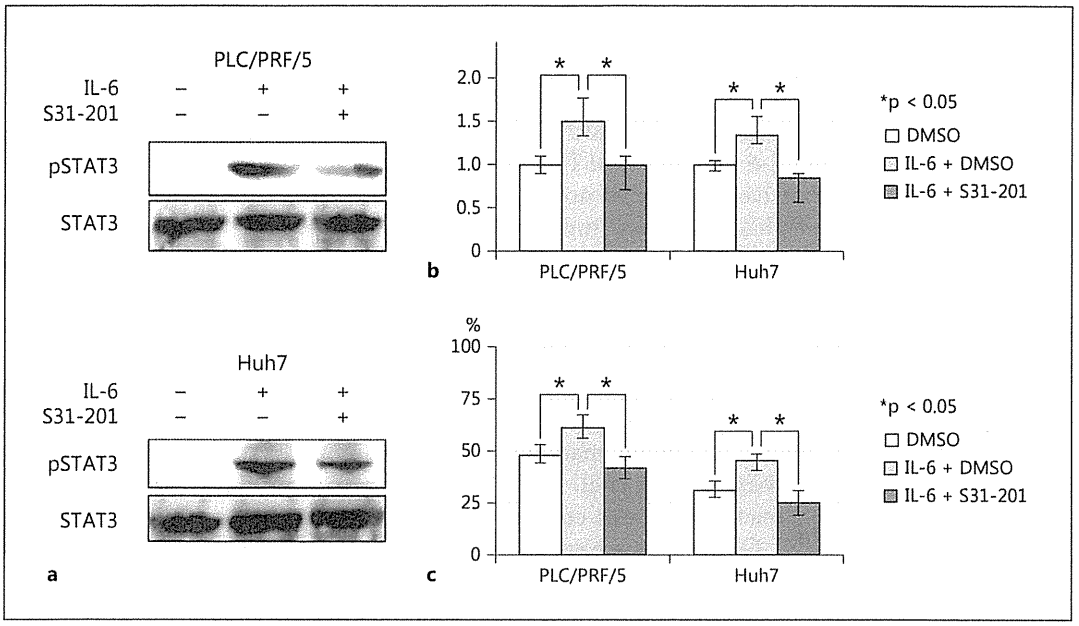

Fig. 4. IL-6 stimulation activated STAT3 signaling and promoted cell proliferation and migration in HCC cell lines. **a** PLC/PRF/5 (upper panel) and Huh7 (lower panel) were treated with 25 ng/ml IL-6 for 30 min. **b** PLC/PRF/5 and Huh7 were cultured with 25 ng/ml IL-6, 100 nM S3I-201 and conditioned medium (1% FBS); cell proliferation was evaluated 48 h after IL-6 stimulation. Control set at 1. **c** PLC/PRF/5 and Huh7 were cultured with 25 ng/ml IL-6, 100 nM S3I-201 and conditioned medium (1% FBS), and wound-healing assay was evaluated 48 h thereafter.

201, a STAT3 inhibitor, inhibited IL-6-induced STAT3 phosphorylation (fig. 4a) and decreased proliferation and migration of HCC cell lines (fig. 4b, c).

Discussion

Our results suggest that macrophage infiltration into HCC tissue stimulates tumor cells via STAT3 signaling. In the present study, pSTAT3-positive HCCs show malignant behavior and confer poor prognosis because of their high abilities of cell proliferation and migration. We found that high pSTAT3 expression was significantly correlated with larger tumor size, higher Ki-67 LI, higher Bcl-XL expression and greater frequency of IMs, and higher pSTAT3 expression was observed in the lesions of IMs and PVIs than in the primary lesions. STAT3 activation upregulates cell cycle-related, antiapoptotic and invasion genes [8–13, 26, 27]. In our results, large tumor size and high Ki-67 LI indicated cell cycle progression, high Bcl-XL expression indicated antiapoptotic function, and frequent IMs indicated invasive capacity. Furthermore, high pSTAT3 expression in the lesions of IMs and PVIs suggests that the tumor cells with STAT3 activation in the primary lesions tended to invade the vessels and metastasize to the other liver sites. Xie et al. [26, 27] reported that activated STAT3 regulated tumor invasion of melanoma cells by regulating the gene transcription of matrix metalloproteinase 2. These results suggest that pSTAT3 expression plays an important role for cell survival and migration in HCC, consistent with previous studies in HCC [14, 17, 28, 29] and other tumors [5, 8–12, 26, 27, 30].

In recent years, it has been recognized that the balance between tumor immunity and tumor progression is important [31]. The present study revealed that tumor-associated macrophages are important for pSTAT3 expression of tumor cells. First, CD163-positive cells around pSTAT3-positive HCC cells were statistically more prevalent than around pSTAT3-negative HCC cells. Some of the CD163-positive cells expressed IL-6 in HCC tissue, and STAT3 was phosphorylated by IL-6 stimulation in vitro. These results suggest that tumor-associated macrophages can activate HCC cells via STAT3 signaling by IL-6 expression. However, CD-163-positive cells were detected not only in the pSTAT3-negative tumor area but

also in the pSTAT3-positive tumor area and in noncancerous liver tissue. IL-6-secreting tumor-associated macrophages may be part of the CD163-positive cells, and the CD163-positive cells in the pSTAT3-positive tumor area were more stained by IL-6 than in the pSTAT3-negative tumor area and normal liver tissue (data not shown). Tumor-associated macrophages express immunosuppressive cytokines including IL-4, IL-6, IL-10, IL-17, and IL-23 [32, 33]. These cytokines activate immunosuppressive inflammatory cells such as other tumor-associated macrophages, helper T cells and regulatory T cells and suppress antitumor inflammatory cells such as lymphocytes, natural killer cells and dendritic cells [34–36]. Kuang et al. [32] showed that tumor-associated macrophages expressed IL-6 in vitro, whereas Ding et al. [21] reported that tumor-associated macrophage was correlated with poor prognosis in HCC. Our results are consistent with these previous reports.

Both proliferation and migration of PLC/RPF/5 and Huh7 were increased following IL-6 stimulation and STAT3 phosphorylation. On the other hand, IL-6 was expressed in not only macrophages but also in HCC cells. STAT3 can be activated through autocrine signaling in HCC cells; moreover, other cytokines and growth factors might activate STAT3 of tumor cells [22–24]. It is very difficult to exclude activation of STAT3 by the autocrine manner. In our data, STAT3 activation of HCC cells was not correlated with surrounding IL-6-positive normal hepatocytes and HCC cells but it was correlated with the infiltration of CD-163-positive cells (fig. 2). Thus, we thought that the IL-6 secretion of tumor-associated macrophages is more important for STAT3 activation of HCC cells than the IL-6 secretion of other cells.

Recently, STAT3 phosphorylation inhibitors such as S3I-201 have been investigated in vitro and in vivo [28–30]. Avella et al. [37] reported that STAT3 can be one of the targets of chemoimmunotherapies. In our study, S3I-201 inhibited IL-6-induced STAT3 phosphorylation in vitro and decreased cell proliferation and migration. The inhibition of tumor-associated macrophages as therapeutic strategy of malignancy has been investigated, too [38–41]. Therefore, it is very important to suppress tumor-associated macrophage activation and STAT3 signaling in the treatment of HCC. Furthermore, tumor-associated macrophage activation requires STAT3 signaling [22]. We consider that the STAT3 inhibitor may suppress STAT3 activation in both tumor cells and tumor-associated macrophages, release antitumor immune systems from suppression by tumor-associated macrophages and thereby control tumor progression of HCC. Therefore, STAT3 signaling is a feasible therapeutic target for HCC.

In conclusion, STAT3 activation is one of the prognostic factors in HCC. Tumor-associated macrophage expresses IL-6 and can activate STAT3 signaling of HCC cells, resulting in their cell proliferation, antiapoptosis and migration. In the future, HCC may be suppressed by inhibition of STAT3 signaling of tumor cells and tumor-associated macrophages.

Disclosure Statement

The authors have no conflicts of interest.

References

1 Llovet JM, Burroughs A, Bruix J: Hepatocellular carcinoma. Lancet 2003;362:1907–1917.
2 Shirabe K, Kanematsu T, Matumata T, Adachi E, Akazawa K, Sugimachi K: Factors linked to early recurrence of small hepatocellular carcioma after hepatectomy: univariate and multivariate analyses. Hepatology 1991; 14:802–805.
3 Taura K, Ikai I, Hatano E, Fujii H, Uyama N, Shimahara Y: Implication of frequent local ablation therapy for intrahepatic recurrence in prolonged survival of patients with hepatocellular carcinoma undergoing hepatic resection: an analysis of 610 patients over 16 years old. Ann Surg 2006;244:265–273.
4 Llovet JM, Ricci S, Mazzaferro V, Hilgard P, Gane E, Blanc JF, de Oliveira AC, Santoro A, Raoul JL, Forner A, Schwartz M, Porta C, Zeuzem S, Bolondi L, Greten TF, Galle PR, Seitz JF, Borbath I, Häussinger D, Giannaris T, Shan M, Moscovici M, Voliotis D, Bruix J, SHARP Investigators Study Group: Sorafenib in advanced hepatocellular carcinoma. N Engl J Med 2008;359:378–390.
5 Bromberg JF, Wrzeszczynska MH, Devgan G, Zhao Y, Pestell RG, Albanese C, Darnell JE Jr: Stat3 as an oncogene. Cell 1999;98:295–303.
6 Al Zaid Siddiquee K, Turkson J: STAT3 as a target for inducing apoptosis in solid and hematological tumors. Cell Res 2008;18:254–267.
7 Murray PJ: The JAK-STAT signaling pathway: input and output integration. J Immunol 2007;178:2623–2629.
8 Berishaj M, Gao SP, Ahmed S, Leslie K, Al-Ahmadie H, Gerald WL, Bornmann W, Bromberg JF: Stat3 is tyrosine-phosphorylated through the interleukin-6/glycoprotein 130/Janus kinase pathway in breast cancer. Breast Cancer Res 2007;9:R32.

9 Lin Q, Lai R, Chirieac LR, Li C, Thomazy VA, Grammatikakis I, Rassidakis GZ, Zhang W, Fujio Y, Kunisada K, Hamilton SR, Amin HM: Constitutive activation of JAK3/STAT3 in colon carcinoma tumors and cell lines: inhibition of JAK3/STAT3 signaling induces apoptosis and cell cycle arrest of colon carcinoma cells. Am J Pathol 2005;167:969–980.

10 Song L, Turkson J, Karras JG, Jove R, Haura EB: Activation of Stat3 by receptor tyrosine kinases and cytokines regulates survival in human non-small cell carcinoma cells. Oncogene 2003;22:4150–4165.

11 Greten FR, Weber CK, Greten TF, Schneider G, Wagner M, Adler G, Schmid RM: Stat3 and NF-kappaB activation prevents apoptosis in pancreatic carcinogenesis. Gastroenterology 2002;123:2052–2063.

12 Ni Z, Lou W, Leman ES, Gao AC: Inhibition of constitutively activated Stat3 signaling pathway suppresses growth of prostate cancer cells. Cancer Res 2000;60:1225–1228.

13 Kreis S, Munz GA, Haan S, Heinrich PC, Behrmann I: Cell density dependent increase of constitutive signal transducers and activators of transcription 3 activity in melanoma cells is mediated by Janus kinases. Mol Cancer Res 2007;5:1331–1341.

14 Rajendran P, Ong TH, Chen L, Li F, Shanmugam MK, Vali S, Abbasi T, Kapoor S, Sharma A, Kumar AP, Hui KM, Sethi G: Suppression of signal transducer and activator of transcription 3 activation by butein inhibits growth of human hepatocellular carcinoma in vivo. Clin Cancer Res 2011;17:1425–1439.

15 Yang SF, Wang SN, Wu CF, Yeh YT, Chai CY, Chunag SC, Sheen MC, Lee KT: Altered p-STAT3 (Tyr705) expression is associated with histological grading and intratumour microvessel density in hepatocellular carcinoma. J Clin Pathol 2007;60:642–648.

16 Ogata H, Kobayashi T, Chinen T, Takaki H, Sanada T, Minoda Y, Koga K, Takaesu G, Maehara Y, Iida M, Yoshimura A: Deletion of the SOCS3 gene in liver parenchymal cells promotes hepatitis-induced hepatocarcinogenesis. Gastroenterology 2006;131:179–193.

17 Pollard JW: Tumour-educated macrophages promote tumour progression and metastasis. Nat Rev Cancer 2004;4:71–78.

18 Lewis CE, Pollard JW: Distinct role of macrophages in different tumor microenvironments. Cancer Res 2006;66:605–612.

19 Hasita H, Komohara Y, Okabe H, Masuda T, Ohnishi K, Lei XF, Beppu T, Baba H, Takeya M: Significance of alternatively activated macrophages in patients with intrahepatic cholangiocarcinoma. Cancer Sci 2010;101:1913–1919.

20 Siveen KS, Kuttan G: Role of macrophages in tumor progression. Immunol Letter 2009;123:97–102.

21 Ding T, Xu J, Wang F, Shi M, Zhang Y, Li SP, Zheng L: High tumor-infiltrating macrophage density predicts poor prognosis in patients with primary hepatocellular carcinoma after resection. Hum Pathol 2009;40:381–389.

22 Fujiwara Y, Komohara Y, Ikeda T, Takeya M: Corosolic acid inhibits glioblastoma cell proliferation by suppressing the activation of signal transducer and activator of transcription-3 and nuclear factor-kappa B in tumor cells and tumor-associated macrophages. Cancer Sci 2011;102:206–211.

23 Takaishi K, Komohara Y, Tashiro H, Ohtake H, Nakagawa T, Katabuchi H, Takeya M: Involvement of M2-polarized macrophages in the ascites from advanced epithelial ovarian carcinoma in tumor progression via Stat3 activation. Cancer Sci 2010;101:2128–2136.

24 Domínguez-Soto A, Sierra-Filardi E, Puig-Kröger A, Pérez-Maceda B, Gómez-Aguado F, Corcuera MT, Sánchez-Mateos P, Corbí AL: Dendritic cell-specific ICAM-3-grabbing nonintegrin expression on M2-polarized and tumor-associated macrophages is macrophage-CSF dependent and enhanced by tumor-derived IL-6 and IL-10. J Immunol 2011;186:2192–2200.

25 Komohara Y, Ohnishi K, Kuratsu J, Takeya M: Possible involvement of the M2 anti-inflammatory macrophage phenotype in growth of human gliomas. J Pathol 2008;216:15–24.

26 Xie TX, Wei D, Liu M, Gao AC, Ali-Osman F, Sawaya R, Huang S: Stat3 activation regulates the expression of matrix metalloproteinase-2 and tumor invasion and metastasis. Oncogene 2004;23:3550–3560.

27 Xie TX, Huang FJ, Aldape KD, Kang SH, Liu M, Gershenwald JE, Xie K, Sawaya R, Huang S: Activation of Stat3 in human melanoma promotes brain metastasis. Cancer Res 2006;66:3188–3196.

28 Lin L, Amin R, Gallicano GI, Glasgow E, Jogunoori W, Jessup JM, Zasloff M, Marshall JL, Shetty K, Johnson L, Mishra L, He AR: The STAT3 inhibitor NSC 74859 is effective in hepatocellular cancers with disrupted TGF-beta signaling. Oncogene 2009;28:961–972.

29 Choudhari SR, Khan MA, Harris G, Picker D, Jacob GS, Block T, Shailubhai K: Deactivation of Akt and STAT3 signalling promotes apoptosis, inhibits proliferation, and enhances the sensitivity of hepatocellular carcinoma cells to an anticancer agent, Atiprimod. Mol Cancer Ther 2007;6:112–121.

30 Lin L, Hutzen B, Zuo M, Ball S, Deangelis S, Foust E, Pandit B, Ihnat MA, Shenoy SS, Kulp S, Li PK, Li C, Fuchs J, Lin J: Novel STAT3 phosphorylation inhibitors exhibit potent growth-suppressive activity in pancreatic and breast cancer cells. Cancer Res 2010;70:2445–2454.

31 Korangy F, Höchst B, Manns MP, Greten TF: Immune responses in hepatocellular carcinoma. Dig Dis 2010;28:150–154.

32 Kuang DM, Peng C, Zhao Q, Wu Y, Chen MS, Zheng L: Activated monocytes in peritumoral stroma of hepatocellular carcinoma promote expansion of memory T helper 17 cells. Hepatology 2010;51:154–164.

33 Kortylewski M, Xin H, Kujawski M, Lee H, Liu Y, Harris T, Drake C, Pardoll D, Yu H: Regulation of the IL-23 and IL-23 balance by Stat3 signaling in the tumor microenvironment. Cancer Cell 2009;15:114–123.

34 Kuang DM, Zhao Q, Peng C, Xu J, Zhang JP, Wu C, Zheng L: Activated monocytes in peritumoral stroma of hepatocellular carcinoma foster immune privilege and disease progression through PD-L1. J Exp Med 2009;206:1327–1337.

35 Wu K, Kryczek I, Chen L, Zou W, Welling TH: Kupffer cell suppression of CD8+ T cells in human hepatocellular carcinoma is mediated by B7-H1/programmed death-1 interactions. Cancer Res 2009;69:8067–8075.

36 Niemand C, Nimmesgern A, Haan S, Fischer P, Schaper F, Rossaint R, Heinrich PC, Müller-Newen G: Activation of STAT3 by IL-6 and IL-10 in primary human macrophages is differentially modulated by suppressor of cytokine signaling 3. J Immunol 2003;170:3263–3272.

37 Avella DM, Li G, Schell TD, Liu D, Zhang SS, Lou X, Berg A, Kimchi ET, Tagaram HR, Yang Q, Shereef S, Garcia LS, Kester M, Isom HC, Rountree CB, Staveley-O'Carroll KF: Regression of established hepatocellular carcinoma is induced by chemoimmunotherapy in an orthotopic murine model. Hepatology 2012;55:141–152.

38 Zhang W, Zhu XD, Sun HC, Xiong YQ, Zhuang PY, Xu HX, Kong LQ, Wang L, Wu WZ, Tang ZY: Depletion of tumor-associated macrophages enhances the effect of sorafenib in metastatic liver cancer models by antimetastatic and antiangiogenic effects. Clin Cancer Res 2010;16:3420–3430.

39 Luo Y, Zhou H, Krueger J, Kaplan C, Lee SH, Dolman C, Markowitz D, Wu W, Liu C, Reisfeld RA, Xiang R: Targeting tumor-associated macrophages as a novel strategy against breast cancer. J Clin Invest 2006;116:2132–2141.

40 Huang Y, Snuderl M, Jain RK: Polarization of tumor-associated macrophages: a novel strategy for vascular normalization and antitumor immunity. Cancer Cell 2011;19:1–2.

41 Wu WY, Li J, Wu ZS, Zhang CL, Meng XL: STAT3 activation in monocytes accelerates liver cancer progression. BMC Cancer 2011;11:506.

ANTIOXIDANTS & REDOX SIGNALING
Volume 00, Number 00, 2013

DOI: 10.1089/ars.2013.5381

ORIGINAL RESEARCH COMMUNICATION

Nitrosative Stress Induces Peroxiredoxin 1 Ubiquitination During Ischemic Insult *via* E6AP Activation in Endothelial Cells Both *In Vitro* and *In Vivo*

Rong-Rong Tao,[1,*] Huan Wang,[1,*] Ling-Juan Hong,[1] Ji-Yun Huang,[1] Ying-Mei Lu,[2] Mei-Hua Liao,[1] Wei-Feng Ye,[1,3] Nan-Nan Lu,[1] Dan-Yan Zhu,[1] Qian Huang,[4] Kohji Fukunaga,[5] Yi-Jia Lou,[1] Ikuo Shoji,[6] Christopher Stuart Wilcox,[7] En-Yin Lai,[4,7] and Feng Han[1]

Abstract

Aims: Although there is accumulating evidence that increased formation of reactive nitrogen species in cerebral vasculature contributes to the progression of ischemic damage, but the underlying molecular mechanisms remain elusive. Peroxiredoxin 1 (Prx1) can initiate the antioxidant response by scavenging free radicals. Therefore, we tested the hypothesis that Prx1 regulates the susceptibility to nitrosative stress damage during cerebral ischemia *in vitro* and *in vivo*. ***Results:*** Proteomic analysis in endothelial cells revealed that Prx1 was upregulated after stress-related oxygen–glucose deprivation (OGD). Although peroxynitrite upregulated Prx1 rapidly, this was followed by its polyubiquitination within 6 h after OGD mediated by the E3 ubiquitin ligase E6-associated protein (E6AP). OGD colocalized E6AP with nitrotyrosine in endothelial cells. To assess translational relevance *in vivo*, mice were studied after middle cerebral artery occlusion (MCAO). This was accompanied by Prx1 ubiquitination and degradation by the activation of E6AP. Furthermore, brain delivery of a lentiviral vector encoding *Prx1* in mice inhibited blood–brain barrier leakage and neuronal damage significantly following MCAO. ***Innovation and Conclusions:*** Nitrosative stress during ischemic insult activates E6AP E3 ubiquitin ligase that ubiquitinates Prx1 and subsequently worsens cerebral damage. Thus, targeting the Prx1 antioxidant defense pathway may represent a novel treatment strategy for neurovascular protection in stroke. *Antioxid. Redox Signal.* 00, 000–000.

Introduction

BRAIN MICROVASCULAR ENDOTHELIAL CELLS provide a barrier between the bloodstream and brain that is critical in brain development, maturation, and homeostasis (9, 37). The balance between endothelial cell survival and death is pivotal for brain remodeling and repair (41). Increased cell death of cerebrovascular endothelial cells exacerbates inflammatory, ischemic, and degenerative brain diseases (26). Before a new strategy can be developed to counter these adverse effects of ischemia-induced endothelial dysfunction and neurovascular damage, it is necessary to define the factors responsible for ischemia-induced blood–brain barrier (BBB) damage.

Under conditions of intense oxidative stress, such as ischemia or hypoxia injury, increased generation of nitric oxide (NO) and superoxide ($O_2^{\bullet -}$) results in the formation of peroxynitrite ($ONOO^-$) (50). This is a short-lived highly reactive oxidant that attacks and inactivates many proteins. Specifically, $ONOO^-$ irreversibly inactivates prostacyclin

[1]Institute of Pharmacology, Toxicology and Biochemical Pharmaceutics, Zhejiang University, Hangzhou, China.
[2]School of Medicine, Zhejiang University City College, Hangzhou, Zhejiang, China.
[3]The Children's Hospital, Zhejiang University School of Medicine, Hangzhou, China.
[4]Department of Physiology, Zhejiang University School of Medicine, Hangzhou, China.
[5]Department of Pharmacology, Graduate School of Pharmaceutical Sciences, Tohoku University, Sendai, Japan.
[6]Division of Microbiology, Center for Infectious Diseases, Kobe University Graduate School of Medicine, Kobe, Japan.
[7]Hypertension, Kidney, and Vascular Research Center, Georgetown University Medical Center, Washington, District of Columbia.
*Both authors contributed equally to this work.

Innovation

Our study is the first demonstration that nitrosative stress initiates the ubiquitination of peroxiredoxin 1 (Prx1) and subsequent disturbance of redox homeostasis in endothelial cells during ischemia-like injury. Our findings further identified E6-associated protein (E6AP) E3 ligase that ubiquitinated Prx1. Thus, repression of peroxynitrite ($ONOO^-$) formation or *E6AP* knockdown dampened the ischemia-induced disturbance of Prx1 defense signaling. Since an active Prx1 was required for optimal neurovascular cell survival, targeting the Prx1 antioxidant defense pathway may represent a novel treatment strategy for neurovascular protection after stroke.

synthase and oxidizes tetrahydrabiopterin to dihydrabiopterin, thereby uncoupling endothelial NO synthase and directing it to generate $O_2^{\bullet -}$ in place of NO. Indeed, endothelial cells are the primary targets of nitrosative stress in cardiovascular disease, stroke, and neurodegenerative disorders (18, 48). Although nitrosative damage to lipids, proteins, and DNA has been implicated in neurovascular damage following cerebral ischemia, the downstream signaling mechanisms remain elusive (13, 16, 17, 29).

Peroxiredoxins (Prxs) are thiol-specific antioxidant enzymes that maintain redox balance under both normal conditions and oxidative stress (6, 7, 10, 28). Although Prx1 is the most abundant and widely distributed member of the mammalian Prxs (23, 24) and is a recognized peroxide-detoxifying enzyme, its pathophysiological role during brain disease remains unclear (38, 44). Cultured *Prx1*-deficient fibroblasts have decreased proliferation and increased sensitivity to oxidative DNA damage. *Prx1*-deficient mice developed hemolytic anemia caused by increased erythrocytic reactive oxygen species (ROS) (34). Furthermore, mutant Hungtington (*mHtt*) gene expression decreased Prx1 levels and increased its sulfonylation (35).

We tested the hypothesis that Prx1 in endothelial cells in culture and in the brain *in vivo* is a pivotal antioxidant pathway but can be damaged by nitrosative stress during hypoxia or ischemia, thereby exacerbating injury. We report that oxygen/glucose-deprived endothelial cells ubiquitinate Prx1 by nitrosative activation of E3 ubiquitin ligase (E6-associated protein [E6AP]). The outcome is that Prx1 is targeted for degradation leading to cellular redox imbalance and loss of the integrity of the endothelial BBB in mice following ischemia. Repression of $ONOO^-$ formation or *E6AP* knockdown dampened these disturbances of Prx1 defense signaling in endothelial cells. The initial study was made in human umbilical vascular endothelial cells, and key observations were confirmed and extended in human brain microvascular endothelial cells (HBMECs). Thus, our results indicate that Prx1 is a pivotal molecule for the protection of endothelial cells and microvessels from ischemia-induced neurovascular damage both *in vitro* and *in vivo*.

Results

Identification of differentially expressed proteins after oxygen–glucose deprivation in endothelial cells

Two-dimensional gel electrophoresis was performed in EA.hy926 endothelial cells to identify proteins that were differentially expressed between control and oxygen–glucose deprivation (OGD)-treated endothelial cells. Figure 1A shows a silver-stained two-dimensional gel electrophoresis reference map of the OGD-treated endothelial cultures (Fig. 1A, $n=3$, lower) in comparison to the control profile (Fig. 1A, $n=3$, upper). The spots that showed a twofold or greater difference between treatments were further characterized by trypsin digestion and matrix-assisted laser desorption/ionization (MALDI) time-of-flight (TOF) mass spectrometry. Twenty-two different proteins from 36 spots were identified with high confidence (CI % ranging from 97.5% to 100%) (Supplementary Table S1; Supplementary Data are available online at www.liebertpub.com/ars). The identified proteins were classified into functional groups (Supplementary Fig. S1). We selected Prx1 for further study since it was implicated in oxidation–reduction balance and abundantly increased 2.5-fold after OGD treatment (Supplementary Fig. S2A).

Temporal changes of Prx1 protein levels in endothelial cells after OGD

Immunoblotting studies demonstrated a time-dependent increase in Prx1 over 1–6 h followed by a decline after 12 h (Fig. 1B, C). There was a similar pattern of protein levels of heat shock protein 27 (HSP27) (Fig. 1B, C). Molecular chaperones such as HSP27 can defend against protein misfolding after sublethal stressful stimuli (4). Immunocytochemical experiments demonstrated intracellular localization of Prx1 (Fig. 1D), which increased 6 h after OGD treatment in the cytosol of endothelial cells (Fig. 1D, E).

Characterization of OGD-induced Prx1 ubiquitination in endothelial cells

Unexpectedly, our western blot data demonstrated a continual increase in the density of a broad, high-molecular-weight (>118 kDa) band for Prx1 starting 6 h after OGD treatment (Fig. 2A). A similar increase in a high-molecular-weight band (>118 kDa) was detected following OGD treatment after probing with an anti-ubiquitin antibody (Fig. 2B). The OGD-induced ubiquitination of Prx1 was confirmed and extended in HBMECs (Fig. 3 A, B) and mouse cerebral microvascular endothelial cells (bEnd.3) (Supplementary Fig. S2B).

Inhibition of proteosomal uptake with MG132 or lactacystin also increased the high-molecular-weight isoforms of Prx1 (Fig. 2C and Supplementary Fig. S3). Probing with an anti-Prx1 antibody in ubiquitin immunocomplexes from OGD-treated endothelial cells revealed a predominant band larger than 118 kDa (Fig. 2D and Fig. 3C). OGD-induced ubiquitination of Prx1 was confirmed by the immunoprecipitation of Prx1 followed by immunoblotting with an anti-ubiquitin antibody (Fig. 2E and Fig. 3D). Consistently, western blot analysis of cell extracts from OGD-treated cells demonstrated that high-molecular-weight conjugates of Prx1 were significantly reduced in *ubiquitin-K48R*-transfected endothelial cells (Fig. 2F and Fig. 3E, F).

The role of Prx1 during proapoptotic cascades after OGD treatment

Proapoptotic proteins were identified by immunoblotting of EA.hy926 cells transfected with either an empty vector or

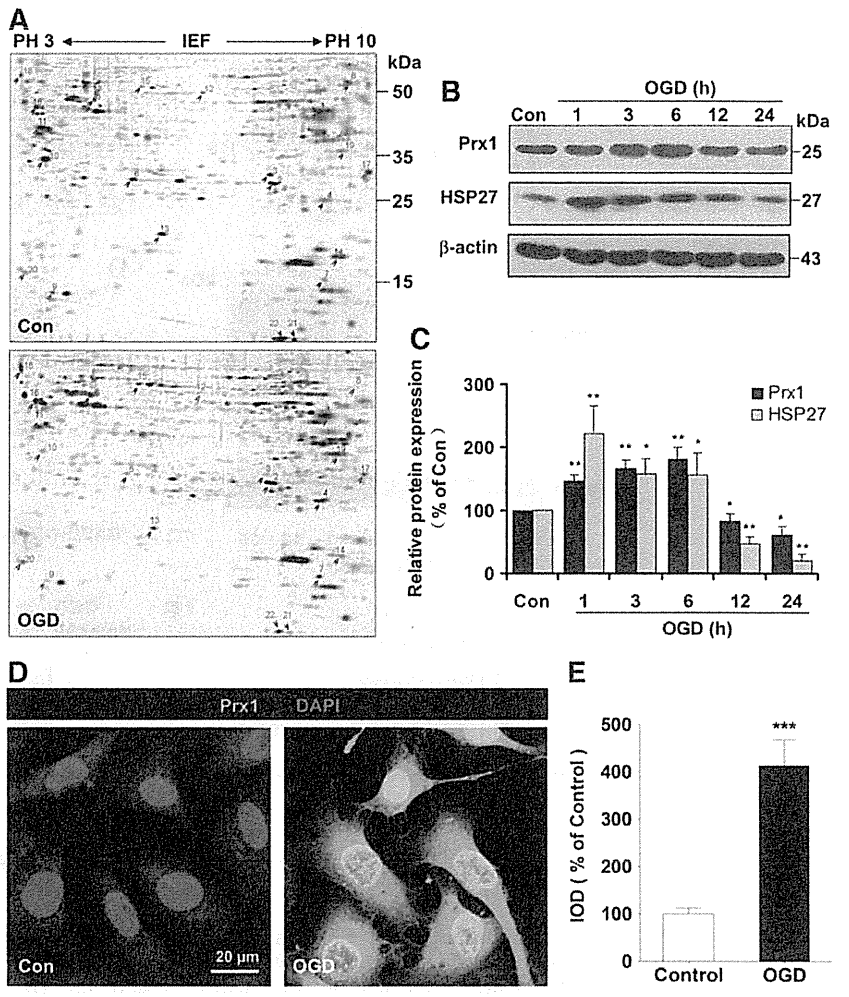

FIG. 1. The proteomic identification of differentially expressed proteins after OGD in endothelial cells. (**A**) Representative silver-stained two-dimensional gel of control and OGD-treated EA.hy926 endothelial cells. Whole proteins (450 μg) were separated on a non-linear pH gradient (3–10) followed by 12% SDS-PAGE. (**B**) Time course of Prx1 and HSP27 protein levels in cell lysates of endothelial cells following OGD. Quantifications of the temporal changes of Prx1 and HSP27 protein levels are shown in (**C**). Immunoblots are representative of three independent experiments. $^{*}p<0.05$; $^{**}p<0.01$ *versus* control. Immunoblotting with an anti-β-actin antibody showed equal amounts of loaded protein in each lane. (**D**) Changes in the immunostaining of Prx1 (green) 6 h after OGD. Subcellular localization of Prx1 was determined by laser confocal microscopy. Data are representative of three independent experiments. Scale bar = 20 μm. (**E**) Quantification of Prx1 immunofluorescence expressed as IOD as described in the Materials and Methods section. $^{***}p<0.001$ *versus* control. IOD, integrated optical density; HSP27, heat shock protein 27; OGD, oxygen–glucose deprivation; Prx1, peroxiredoxin 1; SDS-PAGE, sodium dodecyl sulfate–polyacrylamide gel electrophoresis. To see this illustration in color, the reader is referred to the web version of this article at www.liebertpub.com/ars

a *Prx1* expression vector following OGD insult (Fig. 4). Calnexin is a type I integral endoplasmic reticulum (ER) membrane chaperone involved in folding newly synthesized (glycol) proteins (8). Overexpression of Prx1 significantly inhibited calnexin, PERK, and Ire-1α degradation (Fig. 4A, B) and also inhibited caspase-3 and poly ADP-ribose polymerase (PARP) cleavage (Fig. 4C, D). Exposure of vector-transfected cells to OGD for 6 h decreased the phosphorylation of anti-apoptotic proteins, such as phospho-ERK (Thr202/Tyr204) and phospho-FKHR (Ser256) (forkhead transcription factor Foxo1), and also decreased the protein levels of heme oxygenase-1 (HO-1) but increased the phosphorylation of c-Jun N-terminal kinase (JNK) and P38 (Fig. 4E, F). By contrast, overexpression of *Prx1* after OGD injury resulted in significant upregulation of anti-apoptotic proteins in endothelial cells (Fig. 4E, F). Exposure of vector-transfected cells to OGD for 6 h elevated terminal deoxynucleotidyl transferase dUTP nick end labeling (TUNEL)-positive staining (Fig. 4G, H), whereas overexpression of Prx1 effectively decreased TUNEL staining (Fig. 4G, H). The apoptosis of endothelial cells was determined using flow cytometry with Annexin V-FITC/propidium iodide (PI). In contrast to control cells (2.20%), we found that OGD treatment induced elevation in the fraction of Annexin V/PI-positive cells (49.92%). Moreover, *Prx1* small interfering RNA (siRNA) transduction further exaggerated OGD-induced cell death (Fig. 4I). The present data demonstrate that Prx1 elicits an anti-apoptotic effect after OGD injury in endothelial cells, coinciding with its antioxidant function in the endothelium (31).

E6AP activation contributes to Prx1 stress response after OGD

Since Prx1 has been identified as a novel E6AP-binding protein (33), the present study further elaborates the role of E6AP in ubiquitination of Prx1 during OGD. Representative blots are presented in Figure 5A and show that E6AP was activated following OGD exposure over 1–24 h (Fig. 5A). Similar change of E6AP was confirmed in HBMEC (Supplementary Fig. S4A, B) and bEnd.3 endothelial cells after OGD (Supplementary Fig. S2B). Immunocytochemical analysis of the endothelial cells revealed OGD-induced strong immunoreactivity for E6AP (red fluorescence) that was undetectable in control cells (Fig. 5B–D and Supplementary Fig. S4C, D), which suggests that OGD-induced ubiquitination of Prx1 is associated with E6AP activation.

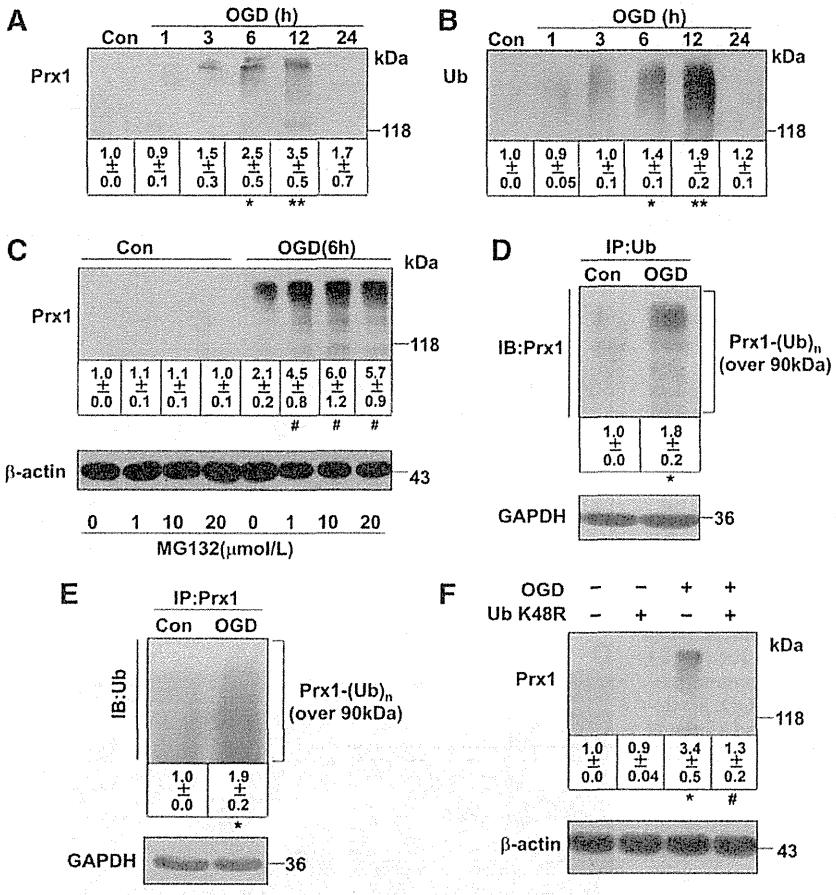

FIG. 2. OGD induces ubiquitination of Prx1 in EA.hy926 endothelial cells. **(A)** Temporal changes in the high-molecular-weight Prx1 isoform were observed in OGD-treated endothelial cells. The accumulated polyubiquitinylated proteins were detected by western blot analysis with anti-Prx1 antibody. **(B)** Protein ubiquitination status after OGD treatment in endothelial cells. The accumulated multiubiquitinylated proteins were detected by western blot analysis with an anti-ubiquitin antibody. **(C)** The changes in polyubiquitinated Prx1 were detected following OGD treatment of endothelial cells with or without proteasome inhibitors. The endothelial cells were treated with 1, 10, or 20 μM MG132 or DMSO 30 min before OGD. The cells were then washed, harvested after 6 h OGD, and analyzed for polyubiquitinated Prx1 levels. **(D)** The OGD-induced ubiquitination of Prx1 was detected by the immunoprecipitation of ubiquitin followed by immunoblotting with an anti-Prx1 antibody. **(E)** Immunoprecipitation of Prx1 from cell lysates of OGD-treated endothelial cells followed by blotting with an anti-ubiquitin antibody. **(F)** The ubiquitin K48R mutant decreased OGD-induced Prx1 ubiquitination in endothelial cells. Endothelial cells were cultured and transfected with plasmid DNA encoding the *ubiquitin-K48R* mutant or an empty plasmid, followed by OGD and immunobloting analysis. Immunoblots are representative of three independent experiments. Data are expressed as the percentage of values of control (mean ± SEM). $^{*}p < 0.05$; $^{**}p < 0.01$ *versus* control; $^{\#}p < 0.05$ *versus* OGD.

E6AP and the active-site cysteine-to-alanine-inactivated mutant E6AP were expressed in mammalian *p3869HA-E6AP C-A* cells (22, 46). Here, after 48 h of transfection, siRNA knockdown of *E6AP* (Fig. 5E, F) or transfection with the *E6AP C-A* mutant (Fig. 5G, H) both significantly blunted the ubiquitination of Prx1 in OGD-treated endothelial cells.

Nitrosative stress associated with the Prx1 defensive response after OGD

The $ONOO^-$ donor 3-morpholinosydnonimine (SIN-1) induced early dose-dependent elevation of Prx1 (Supplementary Fig. S5A, B) and Prx1 ubiquitination (Fig. 6A, B) in endothelial cells as detected by immunoblot, accompanied by increased Prx1 immunostaining (Fig. 6C) and activation of E6AP (Fig. 6D). Whereas increased nitrotyrosine immunostaining and E6AP immunoreactivity were observed in OGD-treated cells (Fig. 6E, F), inhibition of $ONOO^-$ with uric acid markedly reduced both nitrotyrosine and E6AP immunostaining after OGD exposure (Fig. 6E). This was confirmed by western blot (Fig. 6G, H). A similar result was observed in endothelial cells treated with $ONOO^-$ decomposition catalysts (FeTPPS, 1 μM) (Supplementary Fig. S6A, B). E6AP immunoprecipitates from the cell lysates were probed with anti-nitrotyrosine antibody (Fig. 6I). The results

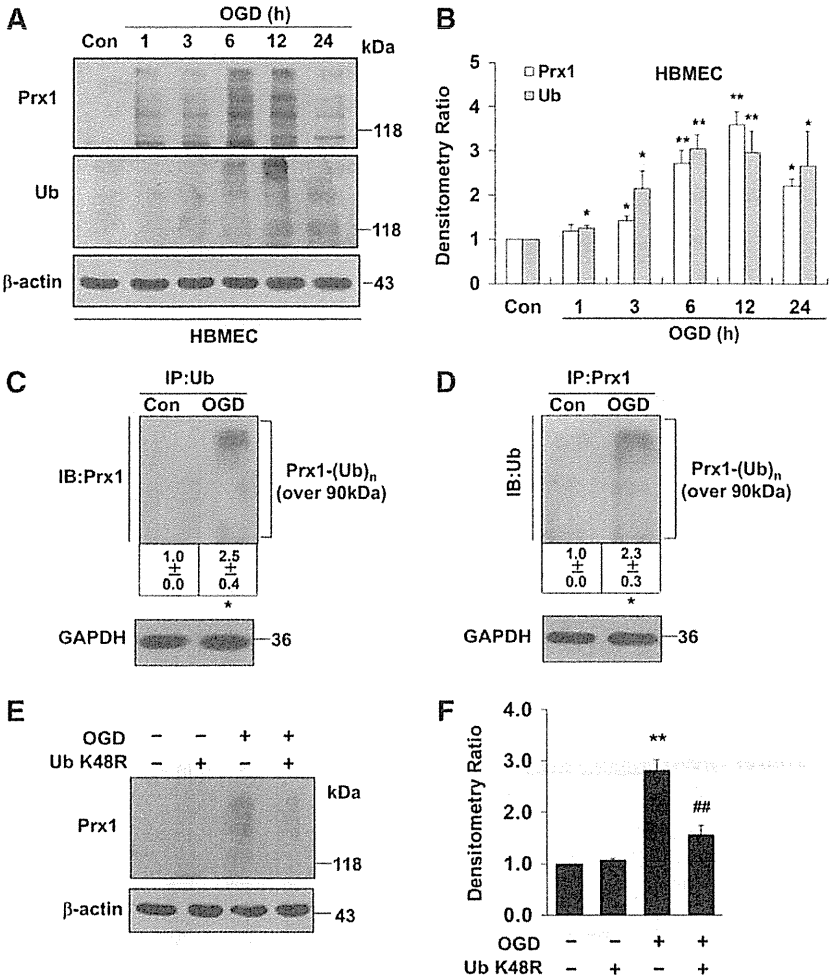

FIG. 3. The ubiquitination of Prx1 in OGD-treated HBMEC. (**A**) The time-dependent change of OGD-induced Prx1 and ubiquitin expression in HBMECs was detected by western blot. (**B**) Densitometry of the western blots for (**A**) was normalized by the level of β-actin as an internal control. (**C**) OGD-treated HBMEC endothelial cells were lysed and subjected to immunoprecipitation with antibodies to ubiquitin. The resultant precipitates were then subjected to immunoblot analysis with antibodies to Prx1. (**D**) Immunoprecipitation of Prx1 from lysed HBMEC with or without OGD treatment were collected for immunoblot analysis with ubiquitin antibody. (**E**) The *ubiquitin-K48R* mutant transfection attenuates Prx1 ubiquitination in OGD-treated endothelial cells. HBMEC were cultured and transfected with plasmid DNA encoding the *ubiquitin-K48R* mutant or an empty plasmid. (**F**) Densitometry of the western blots for (**E**) was normalized by the level of β-actin as an internal control. Immunoblots are representative of three independent experiments. Data are expressed as the percentage of values of control (mean ± SEM). $^{*}p < 0.05$; $^{**}p < 0.01$ *versus* control; $^{\#\#}p < 0.01$ *versus* OGD. HBMEC, human brain microvascular endothelial cell.

demonstrated that the E6AP/nitrotyrosine interaction in OGD-treated endothelial cells was significantly increased. Consistently, OGD-induced tyrosine nitration of E6AP was further confirmed by the immunoprecipitation of nitrotyrosine followed by immunoblotting with an anti-E6AP antibody (Fig. 6J). In addition, Prx1 immunoprecipitates from the lysates were probed with anti-nitrotyrosine antibody demonstrating that OGD did not induce Prx1 protein co-immunoprecipitate with nitrotyrosine (Supplementary Fig. S7). Melatonin blunted the ubiquitination of Prx1 in OGD-treated cells (Supplementary Fig. S8), suggesting that nitrosative stress induced Prx1 ubiquitination during OGD.

E6AP activation contributes to Prx1 stress response in brain microvessels after transient middle cerebral artery occlusion in mice

Since there are limited *in vivo* data on the degradation of Prx1 by ubiquitin ligases in ischemic brain, we used a mouse transient middle cerebral artery occlusion (tMCAO) model for further study. The immunoreactivity for E6AP was observed predominantly in the ipsilateral brain microvessel endothelium 6 h after tMCAO (Fig. 7A-e), accompanied by increased Prx1 immunoreactivity (Fig. 7A-d). A representative Z-stack image is shown in Figure 7B. However, after 24 h, Prx1 was downregulated where E6AP remained upregulated in the brain microvessel endothelium (Fig. 7A, g-i). Ubiquitination of Prx1 was elevated significantly in the brain microvessels 6 h after MCAO (Fig. 7C, D), whereas Prx1 staining was observed in microvessels of sham-operated animals where ubiquitin staining was absent. To further determine E6AP as a key modulator in nitrosative stress-mediated cerebrovascular damage *in vivo*, we stereotaxically delivered a lentivirus carrying mouse sh*E6AP* into the ventricle in mice 2 weeks before MCAO, followed by ischemia and 24 h reperfusion. Western blot analysis showed that lentivirus-mediated cerebral *E6AP* knockdown reduced cerebrovascular damage, which was demonstrated by preventing ischemia-induced dephosphorylation of prosurvival kinases and tight junction proteins breakdown (Fig. 7E–G).

Lentiviral-Prx1 brain transduction protects against neurovascular damage in tMCAO mice

Two weeks after the cerebroventricular injection of a lentiviral-GFP vector encoding mouse *Prx1* (LV-*Prx1*), there was efficient and sustained GFP fluorescence in the brain ventricles (Fig. 8A), cortex (Fig. 8B), hippocampus, and

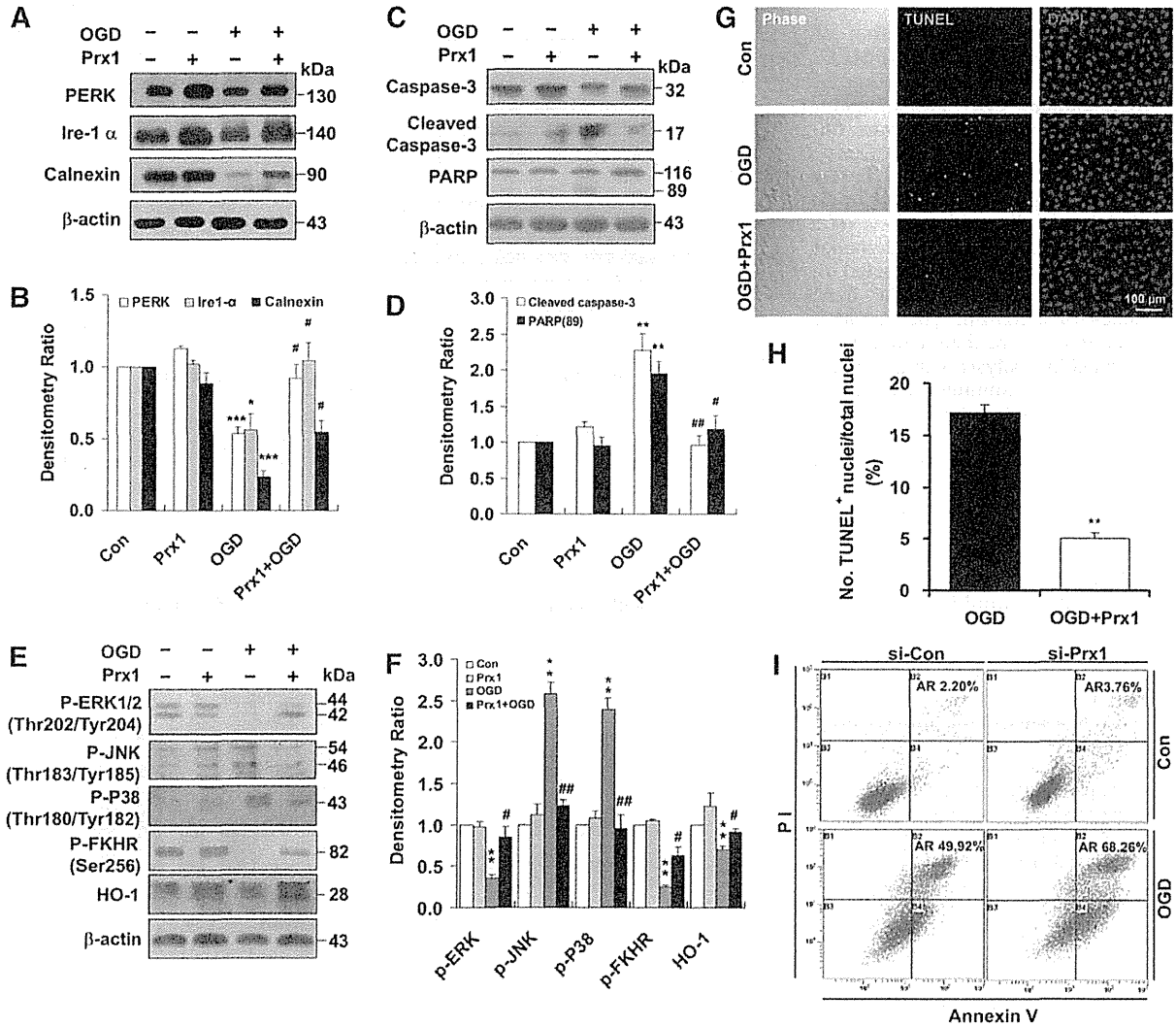

FIG. 4. Role of Prx1 in the OGD-induced apoptotic cascade in endothelial cells. (**A**) The effects of Prx1 on OGD-induced ER stress signaling were determined by immunoblotting. (**B**) Densitometry of western blots for PERK, Ire-1α, and calnexin levels 6 h after OGD, with or without *Prx1* transfection. Data are expressed as densitometry ratio of control (mean ± SEM). $^{*}p < 0.05$; $^{***}p < 0.001$ *versus* control; $^{\#}p < 0.05$ *versus* OGD. (**C**) The effects of Prx1 overexpression on OGD-induced caspase-3 and PARP levels were evaluated by immunoblotting. EA.hy926 cells were cultured and transfected with plasmid DNA encoding *Prx1* or an empty plasmid using Attractene. (**D**) The quantification data for blots are shown in (**C**). Data are expressed as densitometry ratio of control (mean ± SEM). $^{**}p < 0.01$ *versus* control; $^{\#}p < 0.05$; $^{\#\#}p < 0.01$ *versus* OGD. (**E**) The effects of Prx1 overexpression on OGD-induced protein levels were evaluated by immunoblotting. Cells were transfected with *Prx1* plasmid followed by 6 h of OGD or control stimulation. Cell lysates were prepared and resolved by SDS-PAGE. The proteins were immunoblotted with antibodies against phospho-ERK, phospho-JNK, phospho-P38, phospho-FKHR (Ser256), and HO-1. (**F**) Quantitative analysis of protein levels for (**E**) was performed by densitometry. Data are expressed as densitometry ratio of control (mean ± SEM). $^{**}p < 0.01$ *versus* control; $^{\#}p < 0.05$; $^{\#\#}p < 0.01$ *versus* OGD. (**G**) Changes in apoptosis 6 h after OGD were detected using the TUNEL assay. Double staining was performed for TUNEL (green) and DAPI (blue). The representative images show the increased percentage of TUNEL-positive apoptotic endothelial nuclei (green fluorescence) 6 h after OGD. Scale bar = 100 μm. (**H**) Quantification of TUNEL-positive apoptotic endothelial cells with or without *Prx1* transfection. Apoptosis was dramatically reduced following the overexpression of the *Prx1* gene in endothelial cells after OGD. $^{**}p < 0.01$ *versus* OGD group. (**I**) Representative flow cytometric dot plots of apoptotic cells after OGD with or without *Prx1*siRNA transfection. Cultured EA.hy926 cells were stimulated for 6 h with OGD with or without *Prx1*siRNA transfection. Cells were double-stained with Annexin-V and PI and analyzed by FACS. Immunoblots are representative of three independent experiments. β-Actin was used as the loading control. DAPI, 4′,6-diamidino-2-phenylindole; ER, endoplasmic reticulum; HO-1, heme oxygenase-1; JNK, c-Jun N-terminal kinase; PARP, poly ADP-ribose polymerase; siRNA, small interfering RNA; TUNEL, terminal deoxynucleotidyl transferase dUTP nick end labeling; PI, propidium iodide. To see this illustration in color, the reader is referred to the web version of this article at www.liebertpub.com/ars